GEOLOGICA CARPATHICA, OCTOBER 2021, 72, 5, 406–424 https://doi.org/10.31577/GeolCarp.72.5.4

Early–Middle Miocene paleoenvironmental and paleoclimate changes in the Toplica Basin (Serbia) inferred from plant biomarkers, biochemical and elemental geochemical proxies

NIKOLA BURAZER[1,✉], ALEKSANDRA ŠAJNOVIĆ[2], MILICA KAŠANIN-GRUBIN[2], GORDANA GAJICA[2], JOVANA ORLIĆ[1], MARIJA RADISAVLJEVIĆ[3] and BRANIMIR JOVANČIĆEVIĆ[1]

[1]University of Belgrade, Faculty of Chemistry, Studentski trg 12-16, 11000 Belgrade, Serbia; ✉nikola.burazer@gmail.com
[2]University of Belgrade, Institute of Chemistry, Technology, and Metallurgy, Department of Chemistry, Njegoševa 12, 11000 Belgrade, Serbia
[3]University of Belgrade, Faculty of Mining and Geology, Đušina 7, 11000 Belgrade, Serbia

(Manuscript received May 5, 2020; accepted in revised form July 29, 2021; Associate Editor: Júlia Kotulová)

Abstract: The study investigates the influence of alluvial-lacustrine processes and paleoclimate variations on the distribution of terpenoids and unsubstituted Polycyclic Aromatic Hydrocarbons (PAHs). The XRF, ICP-MS, Rock-Eval, and organic geochemical analyses were employed to investigate thirty Lower and Middle Miocene sedimentary samples from the Prebreza and Čučale formations, collected from boreholes BL3 and BL5, situated in the central part of the Toplica Basin (Serbia). The development of the studied basin part was influenced by alluvial-lacustrine processes, which affected the type of organic matter (OM) and the paleoenvironment. Sandy silt and gravel layers in the profile of the BL3 borehole indicate the contribution of thicker clasts brought by rivers. In the BL5 borehole, there are fine-grained intrabasinal lacustrine sediments in the lower part, and swamp sediments in the upper part. The lowest total organic carbon (TOC) content is in alluvial sediments of BL3 and some lacustrine sediments of BL5. Based on Hydrogen Index (HI) and C/N ratio, various mixtures of terrigenous and algal organic matter are present in the sediments, while an increase in the proportion of terrestrial organic matter with higher HI (Type II kerogen) is recorded in upper parts of both boreholes, which may be related to paleoclimatic changes. Based on T_{max}, the OM is immature and/or in the initial stage of maturity. The presence of plant terpenoids and unsubstituted PAHs, which reflected paleoflora and paleoclimate changes, was associated with the suggestion of predominating Type III kerogen in the studied sediments. Various factors influenced the application of gymnosperms/angiosperms parameters. For instance, the progressive aromatization of triterpenoids occurred in the BL5, whereas the process was hindered in the upper part of the BL3, probably as a result of high sedimentation rates. Based on C-value, Sr/Cu, and Rb/Sr ratios, during the deposition of the Lower and Middle Miocene formations of Čučale and Prebreza, a warm and humid climate prevailed, reflecting the Middle Miocene Climatic Optimum (MMCO). The production of unsubstituted PAHs in the studied samples probably relates to paleo-wildfires, anoxic conditions, or the presence of specific biomass precursors.

Keywords: Lower–Middle Miocene paleoclimate, elemental geochemistry, plant terpenoids, Polycyclic Aromatic Hydrocarbons (PAHs), alluvial-lacustrine, Middle Miocene Climatic Optimum (MMCO).

Introduction

A better understanding of early diagenetic pathways of vascular plant biomarkers is important for the paleoenvironmental reconstruction, particularly paleoclimate conditions. Saturated and aromatic vascular plant biomarkers, as well as unsubstituted PAHs, are now widely accepted as molecular tracers for paleoflora and paleoclimate changes (Otto & Wilde 2001; Hautevelle et al. 2006; Xu et al. 2019). Diterpenoids preferentially originate from resins and waxes of gymnosperms, while triterpenoids derive from the root, wood, and bark of most angiosperms (Bechtel et al. 2001, 2003; Otto & Wilde 2001; Hautevelle et al. 2006). The production of unsubstituted PAHs occurs by either diagenetic/catagenetic transformations or the combustion of the plant material (Xu et al. 2019).

The presence of di- and triterpenoids is often related to the OM enriched in Type III kerogen and odd long-chain homologs of *n*-alkanes (Tissot & Welte 1984; Vandenbroucke & Largeau 2007; Bush & McInerney 2013). However, changes in paleoenvironmental conditions determine the presence of vascular biomarkers and PAHs. It is worth mentioning that vascular plant biomarkers are both autochthonous and allochthonous, representing the vegetation of the lake surroundings, while combustion derived PAHs are pre-depositional, resulting from paleo-wildfires, characteristic for environments in which volcanic processes (pyroclastic flows or high temperatures during volcanic eruptions), regional climate changes, or lightning strikes are occasional (Hautevelle et al. 2006; Abarzúa et al. 2016; Xu et al. 2019).

The parameters predicated on the contribution of gymnosperms versus angiosperms should reflect the nature of the climatic variations, by examining which plant taxa become more or less dominant (Bechtel et al. 2001, 2003; Hautevelle et al. 2006; Nakamura et al. 2010). The conifer group of

gymnosperms, as well as angiosperms, may settle in both arid and humid regions (Hautevelle et al. 2006; Zhang et al. 2018). For instance, Hautevelle et al. (2006) have suggested that *Araucariaceae*, *Cupressaceae*, *Podocarpaceae,* and *Taxodiaceae* conifers preferentially settle in humid environments while *Pinaceae* species have acquired many xeromorphic adaptations, allowing them to adapt in both humid and arid regions. Besides, Soclo et al. (2000), Fabiańska & Kurkiewicz (2013), and Xu et al. (2019) suggest that the production of low molecular weight (LMW) unsubstituted PAHs, namely phenanthrene, fluoranthene, and pyrene, results from paleo-wildfires. Moreover, the accumulation of high molecular weight (HMW) unsubstituted PAHs, such as perylene, relates to anoxic environments or the presence of specific precursor biomass (Soma et al. 1996, Bechtel et al. 2007). Nevertheless, the occurrence of gymno- and angiosperms within almost all climate zones, mixed origins of the OM, aromatization of triterpenoids, diagenetic processes, as well as the dynamic of some sedimentological processes during basin development, may complicate the application of these parameters (Wen et al. 2000; Nakamura et al. 2010). A higher abundance of aromatized in comparison to non-aromatized angiosperm triterpenoids could theoretically indicate intense aromatization of triterpenoids during diagenesis. Therefore, the estimation of climate conditions during the depositional period by using inorganic paleoclimate parameters is essential.

Fu et al. (2015), Liu & Zhou (2007), and Xie et al. (2018) have proposed various inorganic parameters, such as the paleoclimate index (C-value), strontium to copper (Sr/Cu), and rubidium to strontium (Rb/Sr) ratio for the paleoclimate reconstruction in distinct paleoenvironments.

One of the most challenging geochemistry tasks is the reconstruction of paleoenvironmental settings, which applies specifically to paleoclimate conditions. A favourable interpretation of the paleoclimate requires the integration of geochemistry, sedimentology, mineralogy, stratigraphy, etc. Moreover, lacustrine environments have complex physical and chemical characteristics, which makes the reconstruction of climate conditions even more challenging, and therefore it is necessary to identify the most reliable paleoclimate parameters (Meyers & Lallier-Verges 1999; Lone et al. 2018).

The study area concerns the Prebreza and Čučale sedimentary series of the Lower/Middle Miocene, deposited in boreholes BL3 and BL5, which are located in the central part of the Toplica Basin, Serbia (Figs. 1, 2). The sediments were selected based on petrological characteristics supported by organic and inorganic geochemistry results. However, this is the first geochemical study of sediments from the central part of this basin. Burazer et al. (2020) have characterized the organic-rich sediments deposited in the north-west part of the Toplica Basin. The OM of these sediments consists mainly of Type II kerogen, deposited in anoxic and mesosaline/hypersaline to mesosaline/freshwater environments.

The study investigates the effect of alluvial-lacustrine processes and paleoclimate variations on the distribution of vascular plant biomarkers, PAHs, and vegetation dynamics. This study has also provided insight into the type and maturity of OM, as well as characteristics of the depositional environment.

Geological settings

The Toplica Basin is located in southern Serbia and is part of the Serbo-Macedonian metallogenic province (Fig. 1a,b; Malešević et al. 1974; Burazer et al. 2020). This basin, covering an area of ~20 km^2, is a north-east–south-west trending intramontane tectonic depression. The central part of this basin is filled with Miocene freshwater limnic, deltaic and swamp sediments, as well as Pliocene and Quaternary freshwater sediments (Malešević et al. 1974). Jurassic diabase on the east, Precambrian metamorphic rocks on the north-east and north, and Cretaceous–Paleogene rocks on the north-east and south surround the basin (Fig. 1c). Upper Cretaceous–Paleogene rocks are represented by breccia, sandstone, conglomerate, sandstone, flysch, claystone, marlstone, and tuffs (Fig. 2; Burazer et al. 2020). The Toplica Basin is a tectonic depression in which longitudinal and diagonal gravitational faults, formed during and after Neogene, have the greatest importance (Malešević et al. 1974). Sediment layers are horizontal or subhorizontal in most parts of the basin. Faults on the western and northern edges, as well as in the middle parts of the depression, are significant for mutual relations of sedimentary formations. On the western edge, near Čučale sedimentary series (Fig. 1c), there is a longitudinal dislocation of the north–south extension, along which the Eggenburgian–Karpatian sediment contact with crystalline shales of the Serbian–Macedonian massif. In the central parts, after the deposition of Sarmatian sediments, several north-west–south-east extension faults were formed, which diagonally intersect the Neogene formations (Malešević et al. 1974).

Furthermore, paleo-alluvial processes influenced the depositional process of studied sediments, particularly in the borehole BL3, in which rivers probably transported and deposited rock fragments that were eroded from the vicinity of the basin (Figs. 1c, 2; Malešević et al. 1974). Alluvial flows have also transported a significant portion of fine-grained andesitic volcanic and volcanoclastic rocks from the Tertiary Lece Magmatic Complex into the basin predominantly from marginal parts (Fig. 2; Malešević et al. 1974; Dragić et al. 2014). Malešević et al. (1974) suggest that the volcanic activity of the Lece Magmatic Complex began in the Late Oligocene and lasted until the Middle Miocene (Fig. 2).

Lithology and stratigraphy

A generalized lithostratigraphic column of the Cenozoic Era of the Toplica Basin, along with lithostratigraphic columns of boreholes BL3 and BL5, are given in Fig. 2. The oldest Eggenburgian–Karpatian Čučale sediments in the borehole BL3 from 670 to 500 m and in the borehole BL5 from 570 to 500 m are represented by clastic sediments, ranging in size

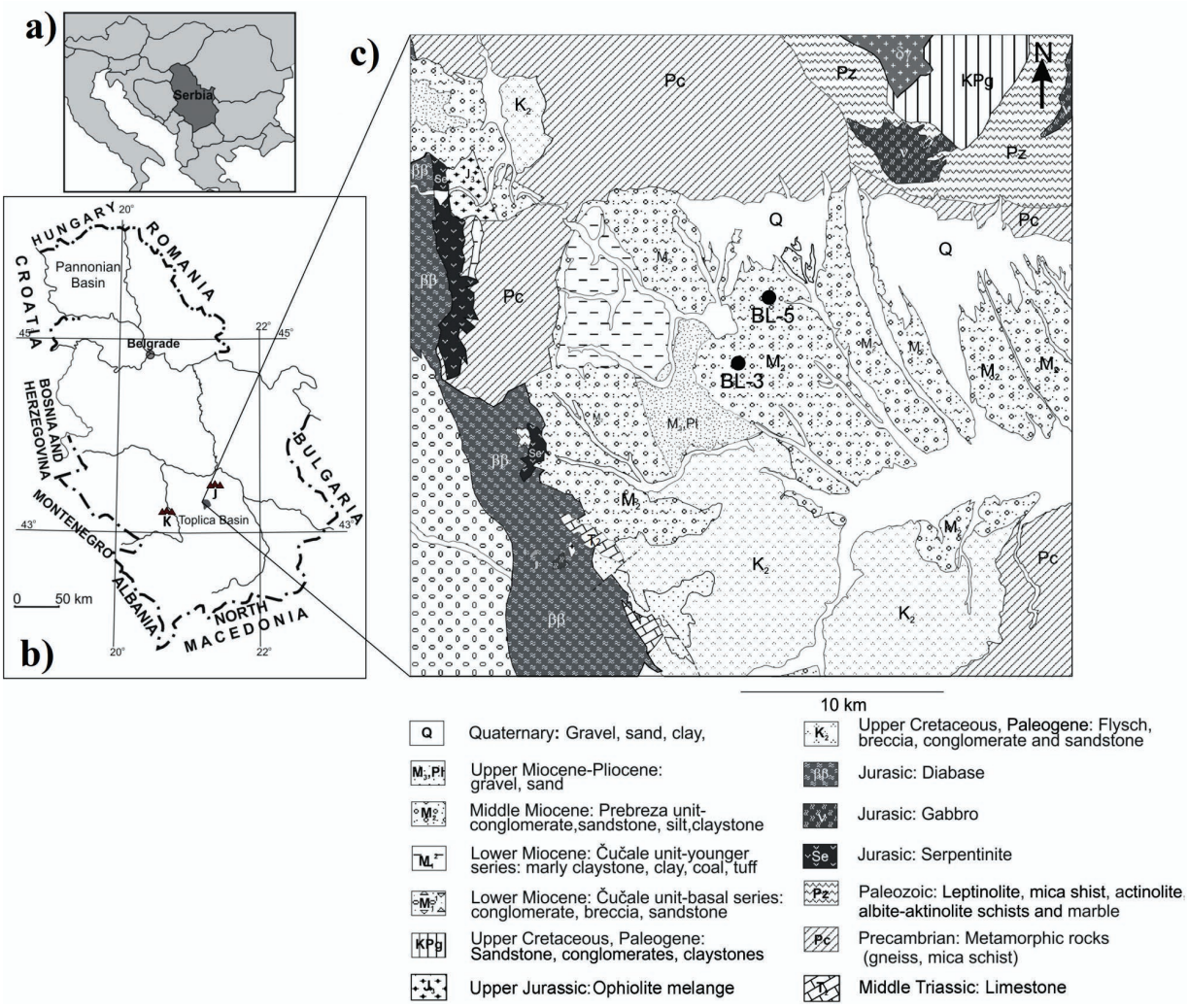

Fig. 1. a, b — Location of the Toplica Basin (latitude from 43°12' to 43°22', longitude from 21°10' to 21°35'; K=Kopaonik, J=Jastrebac). **c** — Simplified geological map with the location of boreholes BL3 and BL5 (modified after Basic Geological Map of Serbia, section L34-031; http://geoliss.mre.gov.rs/OGK/RasterSrbija/).

from silts to gravely sands (Fig. 2). The borehole BL3, 670 m deep, is located in the Middle Miocene unit (M2), represented by conglomerates, sandstones, silts, and claystones (Figs. 1c, 2). Three lithofacies, basin (C-1 and C-2), prodelta (B), and submerged delta (A), can be determined throughout the profile (Table 1). The base of the profile (up to 600 m, lithofacies C-2, Fig. 2) comprises layers of silt sediments deposited in lacustrine conditions (up to 600 m, Fig. 2). Overlying is a section of 300 m thick complex of submerged delta sediments (from 600 to 300 m) represented by silts with layers of sand and gravel (lithofacies A, Table 1, Fig. 2). Sedimentation continues with a hundred metres of prodelta sediments, which are dominantly silts with rare sand and gravel layers (lithofacies B). The Badenian–Sarmatian sedimentation (from 200 to 100 m and above 100 m, respectively) sedimentation ends with lacustrine sediments represented by silts with layers of marls and sands (lithofacies C-1, Fig. 2). They are overlain by coarse sediments deposited in the final lake phase.

Additionally, Figure 1c shows the location of the borehole BL5, situated in the northern part of the central Toplica Basin. Sediments in this borehole are 570 m thick (Fig. 2), which corresponds to two lithofacies: lacustrine (0–185 and 245–570 m) and swamp (185–245 m, Table 1). Above 185 m, poorly sorted sandy medium and coarse grained Sarmatian clastites are present. Coaly clay mixed with fine-grained Badenian sandstones represent Badenian swamp sediments. On the other hand, lacustrine sediments have displayed some lithological variations (Table 1, Fig. 2). The presence of distinctive varieties of Badenian siltstones, mainly clayey, sandy, or marly, characterizes the lacustrine sediments deposited above the depth of 310 and below 370 m. At the depth interval of 315 and 370 m, a layer of iron oxide concretions followed by siltstones, clayey silt, and silty shales, along with a greater or lesser occurrence of carbonate or sandy components, are recorded.

The age determination of sediments from the investigated boreholes relies on the scarce presence of paleontological

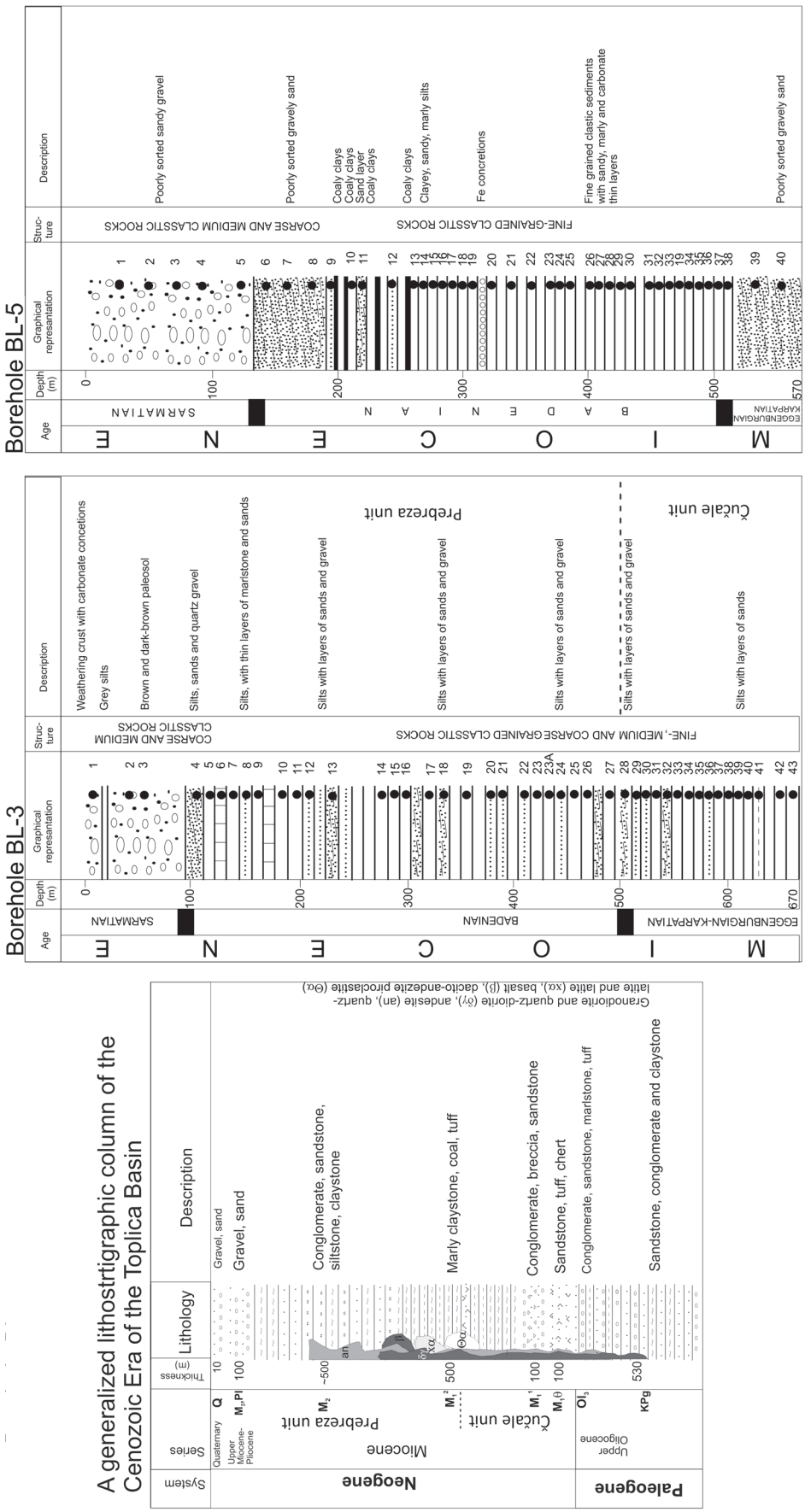

Fig. 2. A generalized lithostratigraphic column of the Toplica Basin with Oligo–Miocene Lece Volcanic Complex in the studed area (**left**), and lithostratigraphic columns of studied boreholes BL3 and BL5 (**right**).

material and sedimentological correlation with previously published data. According to the previous paleontological analysis results (borehole BL5, Ljupko Rundić, personal communication, and unpublished data), the depth interval from 209 to 505 m probably represents one deposition cycle corresponding to lake sedimentation. The finding of the genus *Mediocypris sp.* (sample BL5/28, 409 m) suggests the Middle Miocene and probably the Badenian (Krstić et al. 2012). Furthermore, Pavlović (1969) has determined the Sarmatian age, according to fauna fossil remains of *Dinotherium aff. giganteum* and *Mastodon angustidens* (at approximately 150 m).

Paleogeography

From the paleogeographical perspective, the territory of Serbia belongs to the Central and Eastern Paratethys domains, with the Eastern Paratethys occupying only a small area in eastern Serbia (Ivanov et al. 2011). During the Miocene, either marine environments or freshwater lakes have formed Paratethys (Utescher et al. 2007a). Warm and humid climate conditions mostly characterized the Miocene period, therefore correlating with long-term trends and patterns, namely the Middle Miocene Climate Optimum (Utescher et al. 2007a). The Toplica Basin is located in South Serbia (Fig. 1), between

Table 1: List, unit, depth, lithofacies specification, and the results of XRF measurements (wt. %) and inorganic geochemical parameters of studied samples.

Unit	Sample	Depth (m)	Lithofacies	Na_2O	MgO	Al_2O_3	SiO_2	K_2O	CaO	TiO_2	MnO	Fe_2O_3	C-value [a]	Sr/Cu [b]	Rb/Sr [c]
Prebreza	BL3/5	113		0.04	2.78	10.75	26.97	1.52	11.02	0.51	0.17	7.77	0.52	7.32	0.15
	BL3/6	127		0.03	15.81	2.65	6.46	0.34	24.23	0.10	0.28	1.71	0.05	55.45	0.02
	BL3/8	148	C-1 *	0.10	4.06	14.07	36.01	2.46	4.94	0.66	0.11	6.31	0.56	6.19	0.27
	BL3/9	165		1.99	3.45	12.86	32.88	2.64	6.97	0.65	0.13	5.65	0.39	7.36	0.24
	BL3/10	190		2.34	4.16	12.69	34.01	2.06	9.45	0.60	0.15	5.53	0.32	18.92	0.12
	BL3/11	207	B *	1.95	3.73	10.22	27.63	1.44	18.74	0.48	0.28	4.78	0.20	35.14	0.04
	BL3/16	305		2.57	3.77	14.62	35.19	2.58	4.92	0.67	0.14	7.03	0.52	7.54	0.29
	BL3/25	465	A *	1.92	3.62	15.33	39.74	2.84	3.06	0.70	0.08	7.00	0.62	3.35	0.52
Čučale	BL3/34	567		2.39	3.31	13.75	37.84	2.53	3.92	0.71	0.10	6.43	0.54	5.95	0.33
	BL3/38	602		1.77	3.47	15.56	39.75	2.84	2.73	0.66	0.10	7.10	0.67	4.10	0.50
	BL3/39	611	C-2 *	2.12	3.22	14.97	41.43	2.67	3.26	0.67	0.09	6.38	0.58	4.92	0.37
	BL3/40	637		2.30	3.21	14.71	41.34	2.73	2.77	0.74	0.12	5.69	0.53	6.85	0.33
	minimum			0.03	2.78	2.65	6.46	0.34	2.73	0.10	0.08	1.71	0.05	3.35	0.02
	maximum			2.57	15.81	15.56	41.43	2.84	24.23	0.74	0.28	7.77	0.67	55.45	0.52
	average			1.63	4.55	12.68	33.27	2.22	8.00	0.59	0.15	5.95	0.46	13.59	0.27
Unit	**Sample**	**Depth (m)**	**Lithofacies**	**Na_2O**	**MgO**	**Al_2O_3**	**SiO_2**	**K_2O**	**CaO**	**TiO_2**	**MnO**	**Fe_2O_3**	**C-value**	**Sr/Cu**	**Rb/Sr**
Prebreza	BL5/10	209	Swamp	0.56	3.39	18.24	42.75	2.73	3.74	0.80	0.09	7.93	0.77	4.12	0.51
	BL5/13	245		0.77	3.52	14.76	37.87	1.73	9.57	0.61	0.13	6.18	0.41	5.68	0.23
	BL5/15	260	Lacustrine	0.92	4.65	17.57	43.15	2.36	6.68	0.66	0.09	6.90	0.48	4.75	0.31
	BL5/16	277		1.67	4.68	12.51	32.17	2.33	7.79	0.50	0.14	6.17	0.38	5.88	0.18
	BL5/17	288		1.46	5.00	14.65	39.03	2.45	5.41	0.62	0.10	6.93	0.49	7.83	0.21
	BL5/19	305		3.88	5.31	16.33	40.62	2.59	4.59	0.64	0.12	6.56	0.41	6.78	0.26
	BL5/20	319		1.95	9.95	10.32	24.66	1.38	17.36	0.32	0.27	5.39	0.19	21.79	0.06
	BL5/21	333		3.37	4.88	15.31	38.41	2.49	5.54	0.64	0.11	6.37	0.40	7.65	0.22
	BL5/22	342		0.86	15.18	5.89	12.87	0.80	22.44	0.19	0.39	4.56	0.13	51.43	0.03
	BL5/24	365		2.22	6.05	11.87	28.96	2.47	7.85	0.58	0.15	6.09	0.34	9.75	0.15
	BL5/26	386		2.68	3.56	13.17	32.30	2.63	4.52	0.62	0.12	7.17	0.55	6.54	0.25
	BL5/28	409		2.35	3.19	12.75	31.84	2.84	4.04	0.63	0.12	7.25	0.59	6.66	0.31
	BL5/31	441		3.17	4.70	14.45	32.33	2.30	6.69	0.60	0.14	6.46	0.39	10.02	0.15
	BL5/33	460		2.78	2.55	13.68	32.41	2.62	3.40	0.69	0.12	7.25	0.65	4.69	0.35
	BL5/34	464		3.31	3.55	13.52	33.19	2.47	4.76	0.66	0.12	6.50	0.47	7.00	0.25
	BL5/35	473		0.66	10.24	3.75	9.10	0.63	20.61	0.17	0.26	5.45	0.18	75.26	0.02
	BL5/36	488		2.43	5.48	12.23	29.16	2.25	7.12	0.58	0.16	6.24	0.37	11.02	0.16
	BL5/38	507		2.03	4.84	12.73	31.72	2.36	4.81	0.62	0.10	6.65	0.48	8.10	0.22
	minimum			0.56	2.55	3.75	9.10	0.63	3.40	0.17	0.09	4.56	0.13	4.12	0.02
	maximum			3.88	15.18	18.24	43.15	2.84	22.44	0.80	0.39	7.93	0.77	75.26	0.51
	average			2.06	5.60	12.99	31.81	2.19	8.16	0.56	0.15	6.45	0.43	14.16	0.22

Lithofacies C-1 * (Basin sediments), B * (Prodelta sediments), A * (Submerged delta sediments), and C-2 * (basin sediments) of Prebreza and Čučale lacustrine sediments; [a] C-value (paleoclimate index)=Σ(Fe+Mn+Cr+Ni+V+Co)/Σ(Ca+Mg+Sr+Ba+K+Na) (arid 0–0.20, semi-arid 0.20–0.40, semi-arid/semi-humid 0.40–0.60, semi-humid 0.60–0.80, and humid 0.80–1, Fu et al. 2015); [b] Sr/Cu ratio over 5 reflects cold and arid, whereas Sr/Cu ratio under 5 reflects warm and humid climate conditions (Xie et al. 2018); [c] High Rb/Sr ratio reflects cold and arid, whereas low Rb/Sr ratio reflects warm and humid climate conditions (Xie et al. 2018).

the Jastrebac and Kopaonik mountains. A hilly to mountainous relief, between 350 and 1500 m a.s.l., characterizes the studied area (Perišić et al. 2004). The climate of this northern Balkan province can be described as moderately continental, in which submesophitic woody and plant representatives from *Betulaceae*, *Fagaceae*, and *Ulmaceae* families (located at 600 m a.s.l.) are mostly predominant (Perišić et al. 2004). The mean annual temperature is around 12 °C, while the mean annual precipitation ranges between 650 and 750 mm (RS RHMZ).

Samples and analytical methods

Samples

From different lithological facies of boreholes BL3 and BL5, located in the central part of the Toplica Basin (Table 1, Fig. 1c), thirty selected core samples were collected. Samples were pulverized using a pestle and mortar and then sieved through a 63 μm sieve. Before the analysis, the samples were dried at 105 °C. Only the Soxhlet extraction method did not require the drying step. For a large number of samples (thirteen samples), organic geochemical analyses were done in duplicate to obtain better analytical reliability of the results.

X-Ray Fluorescence (XRF)

Samples and tableting aid wax were mixed in a ratio of 85:15 to prepare them as pressed pellets with the Retsch PP25 hydraulic press. Using an ARL PERFORM'X Sequential X-Ray Fluorescence Spectrometer, semi-quantitative and qualitative analyses were done. Instrument specifications, standards, and the software used to interpret the results have been given in El. Suppl. 1.

Inductively coupled plasma-mass spectrometry (ICP-MS)

The samples were treated with the *aqua regia* solution (HNO_3-HCl, 1:3, v:v) and digested in a microwave furnace for 45 minutes. The resulting solution was diluted using de-ionized water and then mixed and analysed on an ELAN 9000 from PerkinElmer. For the quantitative analysis, the calibration standards included several mixed solutions of high purity elements in 2 % HNO_3. Lake sediment standards (LKSD-1, LKSD-3) and samples were repeatedly measured to monitor the quality of measurements.

Elemental analysis

The samples were treated with diluted hydrochloric acid (1:3, v:v) to eliminate carbonates. Afterward, the elemental analysis (C, H, N, S) with a Vario EL III, CHNS/O Elemental Analyser, Elementar Analysensystem GmbH was performed, using the coal standard (NCS FC 28009L 2016).

Rock-Eval pyrolysis

The Rock-Eval pyrolysis was done with a Rock-Eval 6 instrument. The procedure of this method has been given in El. Suppl. 1.

Organic geochemical analysis

The Soxhlet extraction was performed with an azeotrope mixture of methanol and dichloromethane (1:7.6, v:v) for thirty-six hours. Elemental sulphur was removed by adding copper to the mixture. The saturated and aromatic fractions were isolated from bitumen using column chromatography (adsorbents: SiO_2 and Al_2O_3, eluents: *n*-hexane and benzene). Subsequently, saturated and aromatic fractions were analysed on an Agilent 7890A GC gas chromatograph coupled to an Agilent 5975C mass selective detector. The instrument specifications and software used to interpret the results have been given in El. Suppl. 1. Mass fragmentograms of the saturated fraction used for the interpretation of biomarkers were *m/z* 71 for *n*-alkanes and isoprenoids, *m/z* 125 for β-carotane, *m/z* 215 and *m/z* 217 for steroids, *m/z* 109, *m/z* 123, *m/z* 191, *m/z* 218, and *m/z* 313 for terpenoids. Mass fragmentograms of the aromatic compounds used for the interpretation were *m/z* 219, *m/z* 221, *m/z* 223, *m/z* 233, *m/z* 237, *m/z* 241, *m/z* 274, and *m/z* 292, *m/z* 178, *m/z* 202, *m/z* 228, and *m/z* 252 for substituted and unsubstituted PAHs, respectively.

Results

Major and trace elements

Table 1 shows a wide variation of almost all major elements, yet the contents of Fe_2O_3 are relatively constant in the studied sediments.

The contents of MgO and CaO, along with Al_2O_3 and SiO_2, are positively linearly correlated, with correlation coefficients (r) above 0.74 and 0.99, respectively, in both studied boreholes. This positive linear relationship also exists between the contents of MnO, CaO, and MgO ($r>0.64$) in both boreholes, which may indicate that manganese is present mainly in carbonate minerals. The contents of K_2O, TiO_2, and Fe_2O_3 are positively linearly correlated with Al_2O_3 and SiO_2 ($r>0.76$) in both boreholes, suggesting that potassium, titanium, and iron are present largely in clay minerals.

The parameters, C-value, Sr/Cu, and Rb/Sr, vary in a wide range in all the studied samples (Table 1, Fig. 3). A statistically significant correlation between these parameters is registered ($r>0.83$) in both studied boreholes.

Bulk geochemical parameters and Rock-Eval analysis

Table 2 demonstrates that the total organic carbon (TOC) content averages 1.22 wt. % (BL3) and 0.87 wt. % (BL5). The content of extractable OM (EOM, Table 2, El. Suppl. 2)

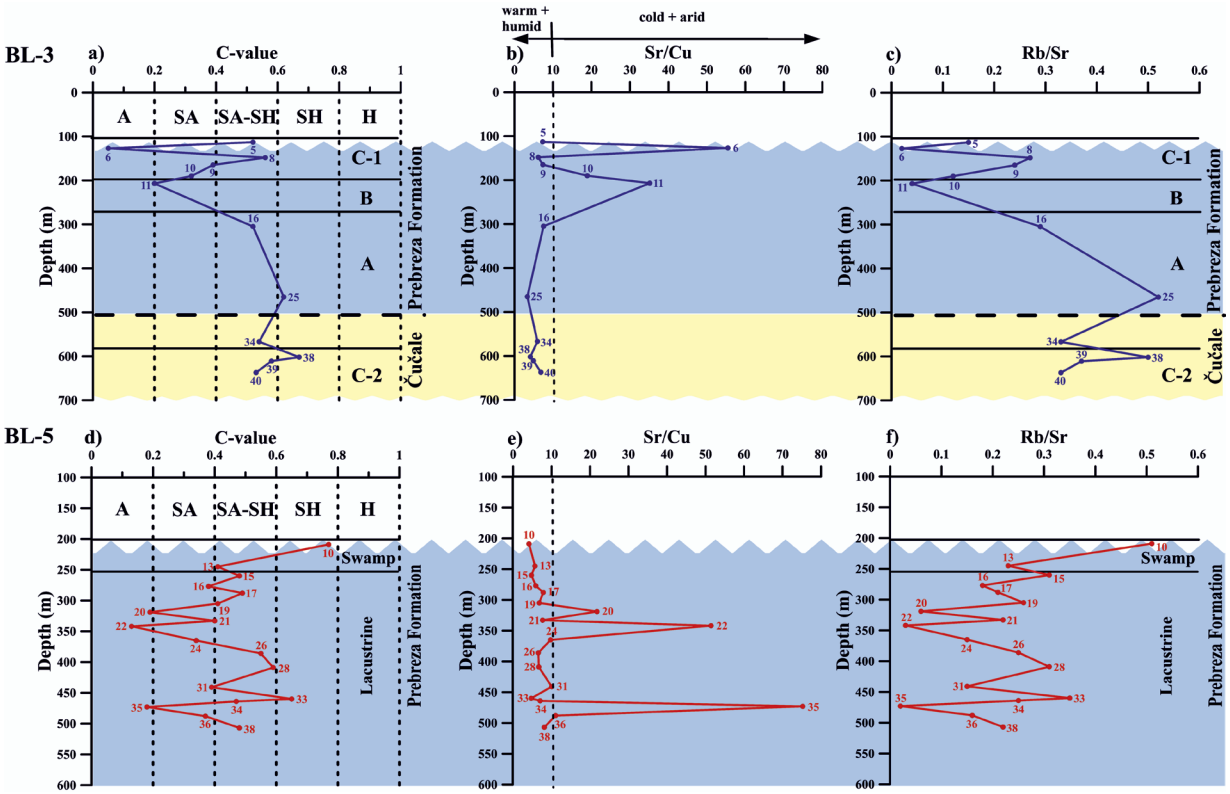

Fig. 3. The C-value ratio (Fu et al. 2015), Sr/Cu (Liu & Zhou 2007), and Rb/Sr (Xie et al. 2018) for sediments of the BL3 (**a–c**) and BL5 (**d–f**). A=arid, SA=semi-arid, SA–SH=semi-arid/semi-humid, SH=semi-humid, H=humid. Facies of BL-3: basinal (C-1 and C-2), prodelta (B), and submerged delta (A).

ranges from 213 to 4571 ppm (BL3) and 164 to 2699 ppm (BL5). The sample BL3/5 has displayed the highest EOM content, which corresponds to the highest value of TOC (Table 2, El. Suppl. 2).

In general, the C/N ratio ranges between 10 and 20 (Table 2, El. Suppl. 3). On the other hand, the C/S ratio is under 10 for a large number of studied samples (El. Suppl. 2).

The content of free hydrocarbons (S1) for most sediments is negligible (Table 2). The content of pyrolysis-derived hydrocarbons (S2) varies in a wide range from 0 to 24.42 (BL3) and from 0.1 to 16.03 (BL5) mg HC/g rock, while the content of organic CO_2 (S3) averages 0.84 (BL3) and 0.67 (BL5) mg CO_2/g rock. The hydrogen HI is generally under 200 mg HC/g TOC (El. Suppl. 3), while the oxygen index (OI) varies between 10 and 487 (BL3), as well as 45 and 235 (BL5) mg CO_2/g TOC. The S2/S3 ratio averages 2.66 (BL3) and 2.70 (BL5). The temperature of maximum hydrocarbon generation (T_{max}) ranges from 358 to 442 °C (BL3) and 421 to 442 °C (BL5).

Molecular composition of OM

n-Alkanes and isoprenoids

Higher proportions of short-chain length (n-C_{17} to n-C_{21}) and odd long-chain length (n-C_{27}, n-C_{29}, and n-C_{31}) n-alkanes, along with the phytane predominance, characterize the saturated lipid fraction of the majority of studied samples (Fig. 4). However, several samples are characterized by dominant mid-chain length n-alkanes, namely n-C_{23} or n-C_{25} (Fig. 4). For most of the samples, the n-alkane maximum (C_{max}) is at n-C_{25}, n-C_{27}, n-C_{29}, or n-C_{31} (Table 3).

The n-C_{27}/n-C_{31} ratio and alkane index (AI=n-C_{31}/(n-C_{31}+n-C_{29})) indicate a general prevalence of n-C_{27} or n-C_{29} over n-C_{31} (Table 3). The n-C_{17}-n-C_{21}/n-C_{27}-n-C_{31} parameter (Table 3) varies from 0.03 to 0.71 (BL3) and 0.15 to 1.40 (BL5). The carbon preference index (CPI index is calculated by using the equation of Bray and Evans for full amplitude of n-alkanes, Tissot & Welte 1984) and terrigenous to aquatic (TAR=(n-C_{27}+n-C_{29}+n-C_{31})/(n-C_{15}+n-C_{17}+n-C_{19})) for several samples are above 2 and 10, respectively (Table 3). The average value of the aquatic macrophytes proxy (P_{aq}= (n-C_{23}+n-C_{25})/(n-C_{23}+n-C_{25}+n-C_{29}+n-C_{31})) is 0.45 and 0.49, for BL3 and BL5, respectively (Table 3). The average chain length (ACL=(25×n-C_{25}+27×n-C_{27}+29×n-C_{29}+31×n-C_{31}+33×n-C_{33})/(n-C_{25}+n-C_{27}+n-C_{29}+n-C_{31}+n-C_{33}), Table 3) parameter averages 28.44 (BL3) and 28.52 (BL5).

The low pristane to phytane (Pr/Ph<1) ratio corroborates the predominance of phytane (Table 3). In contrast to samples of the BL5, lower concentrations of isoprenoids i-C_{25} and i-C_{30}, as well as the absence of β-carotane, characterize samples of the BL3 (Table 3).

Table 2: The results of Rock-Eval and bulk organic geochemical parameters of studied samples.

Sample	TOC [a]	EOM [b]	C/N **	C/S **	S1 [c]	S2 [d]	S3 [e]	HI [f]	OI [g]	S2/S3	T_{max} [h]
BL3/5	6.64	4571	28.19	7.38	0.38	24.42	4.27	368	64	5.72	440
BL3/6 *	0.10	213	15.09	14.53	0.00	0.10	0.49	99	487	0.20	442
BL3/8	1.68	2594	17.62	5.17	0.17	7.74	0.84	460	50	9.21	434
BL3/9	1.26	1659	18.67	5.44	0.11	4.62	0.83	367	66	5.57	431
BL3/10	1.49	389	21.23	2.73	0.18	5.10	0.98	342	66	5.20	429
BL3/11	0.48	333	20.30	3.36	0.00	0.00	0.05	0	10	0.00	N.D [i]
BL3/16	0.99	464	14.23	1.20	0.00	0.00	0.75	0	75	0.00	358
BL3/25	0.19	254	1.83	5.05	0.00	0.01	0.43	5	232	0.02	394
BL3/34	0.18	214	5.25	N.D	0.00	0.06	0.28	34	159	0.21	429
BL3/38	0.18	489	12.13	2.29	0.00	0.07	0.36	39	198	0.19	430
BL3/39	0.50	898	N.D	2.78	0.00	0.53	0.38	107	77	1.39	429
BL3/40	0.89	422	N.D	9.90	0.01	1.90	0.45	213	50	4.22	438
minimum	0.10	213	1.83	1.20	0.00	0.00	0.05	0	10	0.00	358
maximum	6.64	4571	28.19	14.53	0.38	24.42	4.27	460	487	9.21	442
average	1.22	1042	15.45	5.44	0.07	3.71	0.84	170	128	2.66	423
Sample	**TOC**	**EOM**	**C/N**	**C/S**	**S1**	**S2**	**S3**	**HI**	**OI**	**S2/S3**	**T_{max}**
BL5/10	0.56	885	4.67	0.63	0.00	0.33	0.55	59	98	0.60	431
BL5/13	2.97	2699	24.11	9.25	0.11	16.03	1.34	540	45	11.96	442
BL5/15	1.83	2132	11.56	58.13	0.10	7.63	0.92	416	50	8.29	433
BL5/16	0.48	772	8.44	2.01	0.00	0.52	0.38	109	80	1.37	432
BL5/17	0.99	1388	17.32	63.33	0.03	1.73	0.63	175	64	2.75	435
BL5/19	0.94	968	13.22	7.68	0.02	1.85	0.59	198	63	3.14	435
BL5/20	0.84	806	18.16	63.64	0.01	3.95	0.56	470	67	7.05	442
BL5/21	1.15	771	15.53	10.92	0.01	2.56	0.72	222	62	3.56	436
BL5/22	0.38	523	22.10	3.82	0.00	1.20	0.89	317	235	1.35	436
BL5/24	0.85	656	17.31	14.38	0.00	1.08	0.94	127	111	1.15	437
BL5/26	0.43	470	15.40	3.03	0.00	0.15	0.46	35	106	0.33	423
BL5/28	0.39	164	13.77	4.63	0.00	0.10	0.48	26	124	0.21	431
BL5/31	0.70	616	25.43	1.32	0.00	0.48	0.62	68	88	0.77	421
BL5/33	0.38	296	12.60	2.15	0.00	0.13	0.50	34	131	0.26	425
BL5/34	0.54	446	21.23	2.73	0.00	0.37	0.69	69	128	0.54	428
BL5/35	0.45	230	17.60	3.68	0.00	0.51	0.61	112	135	0.84	439
BL5/36	0.76	494	N.D	N.D	0.00	0.44	0.61	58	80	0.72	429
BL5/38	0.92	1592	12.30	4.07	0.02	1.92	0.51	208	55	3.76	427
minimum	0.38	164	4.67	0.63	0.00	0.10	0.38	26	45	0.21	421
maximum	2.97	2699	25.43	63.64	0.11	16.03	1.34	540	235	11.96	442
average	0.87	884	15.93	15.03	0.02	2.28	0.67	180	96	2.70	432

*** Figure 5 has excluded the interpretation of bolded samples, which have low TOC (<0.50 wt. %) or S2 (<0.20 mg HC/g rock), except the sample BL5/16 (TOC near 0.50 wt. % and S2 0.52 mg HC/g rock,** Peters 1986); [a] TOC=total organic carbon (wt. %); [b] EOM=extractable organic matter (ppm); ** molar ratios of C/N and C/S; [c] S1=free hydrocarbons (mg HC/g rock); [d] S2=pyrolyzate hydrocarbons (mg HC/g rock); [e] S3=yield of CO_2 (mg CO_2/g rock); [f] HI=hydrogen index=S2×100/TOC (mg HC/g TOC); [g] OI=oxygen index=S3×100/TOC (mg HC/g TOC); [h] T_{max}=temperature of maximum S2 yield; [i] N.D=Not Determined.

Steroids and terpenoids

Figure 5 shows the distribution and relative abundance of steroid and terpenoid biomarkers (Table 4). Table 5 demonstrates a wide span in values of steroid to hopanoid (S/H) ratio, ranging from 0.19 to 13.30 (BL3) and 0.18 to 12.40 (BL5). A general predominance of C_{29} over C_{27} and C_{28} 5α(H), 14α(H), 17α(H)-20R or $\Delta^2\Delta^4\Delta^5$, steranes or sterenes, characterizes most of the studied samples. The moretane to hopane (C_{30}M/C_{30}H) ratio indicates a slight prevalence of C_{30} βα moretane over C_{30} αβ hopane. The presence of extended moretanes, from C_{31} to C_{35} 17β, 21α(H)-22R, characterizes all the studied samples (Fig. 5a). In general, the C_{31} homohopane ratio is under 0.46 (BL3) and 0.48 (BL5), whereas the C_{29} sterane ratio is under 0.12 in both BL3 and BL5. The values of the gammacerane index (GI) are generally high (GI>1).

Saturated and aromatic terpenoids and unsubstituted PAHs

Table 4 and Figure 5b demonstrate identified saturated and aromatic di- and triterpenoids, as well as PAHs. Consequently, the aliphatic gymnosperms to angiosperms (al-AGR, Table 6) parameter is calculated based on the distribution and relative abundance of saturated terpenoids (compounds listed from 1t to 9t, Table 4), and averages 0.41 (BL3) and 0.57 (BL5). In general, mixed contents of saturated and aromatic triterpenoids characterize samples of BL3 (Table 6), while aromatic triterpenoids predominate in samples of BL5 (avg. of ∑Saturated triterpenoids/∑Aromatic triterpenoids ratio is 0.14, and is calculated based on the distribution and relative abundance of compounds listed from 1t to 23t, Tables 4, 6). Moreover, the aromatic gymnosperms to angiosperms (ar-AGR), aromatic oleananes to gymnosperms (ar-AGR_{ole}),

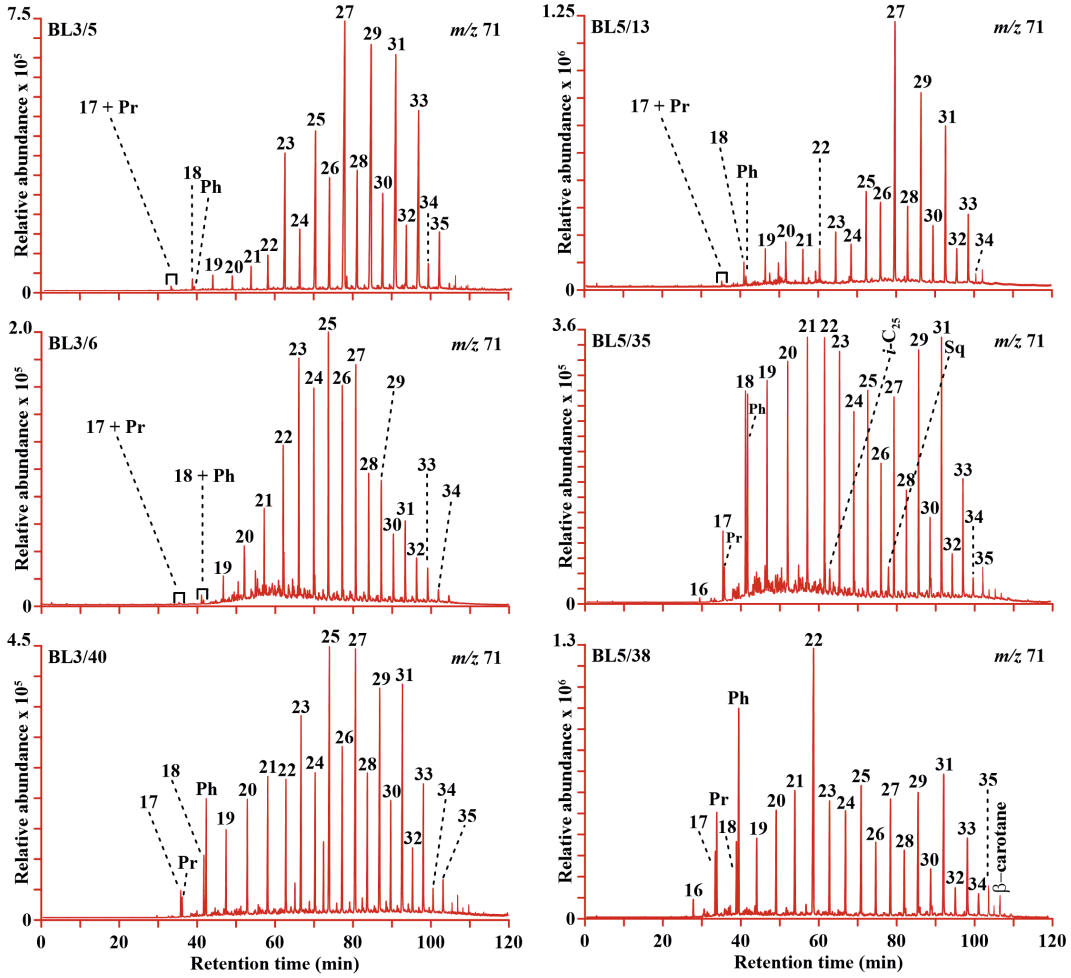

Fig. 4. Fragmentograms of *n*-alkanes and isoprenoids of representative samples BL3/5, BL3/6, BL3/40, BL5/13, BL5/35, and BL5/38 (the number of the peak corresponds to the chain length of *n*-alkane).

saturated and aromatic gymnosperms to angiosperms (al, ar-AGR), $LWM_{PAHs\ (unsubstituted)}/HMW_{PAHs\ (unsubstituted)}$ parameters are calculated based on the distribution and relative abundance of aromatic terpenoids (compounds listed from 10t to 23t, Table 4) and PAHs (compounds listed from 24p–30p, Table 4). Table 6 shows the results of these parameters. The al-AGR and al, ar-AGAR parameters follow the same trend, averaging 0.25 and 0.31 (BL3), along with 0.25 and 0.28 (BL5), respectively. The ar-AGR_{ole} parameter ranges from 0.00 to 0.94 (BL3) and from 0.13 to 0.93 (BL5), while the average values of the $LWM_{PAHs\ (unsubstituted)}/HMW_{PAHs\ (unsubstituted)}$ parameter are 2.69 (BL3) and 3.00 (BL5), indicating a higher contribution of LMW over HMW PAHs in both studied boreholes.

Discussion

Type of OM

Peters (1986) has pointed out that the reliability of the Rock-Eval parameters for sediments with low TOC (<0.50 wt. %) and S2 (<0.50 wt. % or 0.2 mg HC/g rock) is questionable. This fact particularly concerns sediments of lithofacies A (submerged delta) and B (prodelta) in the borehole BL3, in which rivers have deposited a significant amount of sand and gravel material with particles of OM (Fig. 2). When excluding these sediments from further interpretation, the analytical data is suggesting that the OM of Prebreza sediments (samples BL3/5–10) consists mainly of the Type II kerogen (HI over 300 mg HC/g TOC), while mixed Type III and Type II/III kerogens characterize the OM of Čučale sediments deposited in the BL3 (samples BL3/39 and BL3/40, HI under 200 or between 200 and 300 mg HC/g TOC, Figs. 6a, b and El. Suppl. 3; Vandenbroucke & Largeau 2007). The OM of Prebreza sediments deposited in BL5 contains mainly Type III and Type II/III kerogens (Fig. 6a, b). A general predominance of the Type III kerogen in a large group of studied sediments relates to the inflow of terrestrial material via the alluvial-lacustrine system into the investigated basin area, which is in accordance with sedimentological and lithological data (see the section Geological Settings). On the other hand, most of the sediments from lithofacies C-1 of the BL3, as well as

Table 3: The results of specific organic geochemical parameters of studied samples, calculated from the distribution and relative abundance of *n*-alkanes and isoprenoids, including marked samples with the relative abundance of isoprenoid β-carotane.

Sample	Depth (m)	C_{max}*	*n*-C_{27}/ *n*-C_{31}	AI [a]	*n*-C_{17}–*n*-C_{21}/ *n*-C_{27}–*n*-C_{31}	CPI [b]	TAR [c]	P_{aq} [d]	ACL [e]	Pr/Ph [f]	*i*-C_{25}**/ *n*-C_{22}	*i*-C_{30}***/ *n*-C_{26}	The presence of β-carotane (*m/z* 125)
BL3/5	113	*n*-C_{27}	1.38	0.46	0.03	4.08	87.63	0.30	28.98	0.30	N.D [g]	N.D	- [h]
BL3/6	127	*n*-C_{25}	3.09	0.39	0.33	1.29	27.78	0.76	26.99	0.10	0.13	0.05	-
BL3/8	148	*n*-C_{31}	0.58	0.54	0.09	2.88	20.88	0.23	29.39	0.17	N.D	N.D	-
BL3/9	165	*n*-C_{31}	0.59	0.55	0.13	2.58	32.16	0.27	29.34	0.13	N.D	0.03	-
BL3/10	190	*n*-C_{20}	1.16	0.49	0.71	1.38	3.19	0.58	28.17	0.03	0.08	0.06	-
BL3/11	207	*n*-C_{27}	1.28	0.46	0.19	1.21	10.68	0.41	28.47	0.16	0.14	0.05	-
BL3/16	305	*n*-C_{31}	0.79	0.53	0.10	1.74	23.09	0.30	29.03	0.20	N.D	N.D	-
BL3/25	465	*n*-C_{25}	1.44	0.46	0.59	1.31	4.77	0.57	28.04	0.05	0.07	0.07	-
BL3/34	567	*n*-C_{25}	1.56	0.45	0.32	1.30	10.37	0.54	28.05	0.06	0.07	0.05	-
BL3/38	602	*n*-C_{25}	1.17	0.52	0.40	2.04	6.37	0.51	28.30	0.17	0.08	N.D	-
BL3/39	611	*n*-C_{18}	2.04	0.46	0.22	2.20	11.36	0.48	28.19	0.10	N.D	N.D	-
BL3/40	637	*n*-C_{25}	1.24	0.50	0.21	2.10	12.01	0.49	28.32	0.02	N.D	0.08	-
minimum		/	0.58	0.39	0.03	1.21	3.19	0.23	26.99	0.02	0.07	0.03	/
maximum		/	3.09	0.55	0.71	4.08	87.63	0.76	29.39	0.30	0.14	0.08	/
average		/	1.36	0.48	0.28	2.01	20.86	0.45	28.44	0.12	0.10	0.06	/
Sample	**Depth (m)**	**C_{max}**	***n*-C_{27}/ *n*-C_{31}**	**AI**	***n*-C_{17}–*n*-C_{21}/ *n*-C_{27}–*n*-C_{31}**	**CPI**	**TAR**	**P_{aq}**	**ACL**	**Pr/Ph**	***i*-C_{25}/ *n*-C_{22}**	***i*-C_{30}/ *n*-C_{26}**	**The presence of β-carotane (*m/z* 125)**
BL5/10	209	*n*-C_{27}	1.96	0.45	0.21	1.85	11.16	0.52	28.53	0.12	0.05	0.07	-
BL5/13	245	*n*-C_{27}	2.03	0.45	0.15	2.11	10.53	0.33	28.52	0.29	N.D	N.D	-
BL5/15	260	*n*-C_{31}	1.04	0.51	0.28	2.06	6.82	0.41	28.70	0.22	N.D	N.D	-
BL5/16	277	*n*-C_{27}	1.37	0.49	0.29	1.58	7.81	0.50	28.30	0.21	0.04	0.02	-
BL5/17	288	*n*-C_{31}	0.84	0.53	0.39	2.19	4.56	0.44	28.70	0.40	0.13	0.05	-
BL5/19	305	*n*-C_{27}	1.55	0.48	0.42	1.72	3.67	0.52	28.41	0.31	N.D	N.D	-
BL5/20	319	*n*-C_{31}	0.83	0.52	0.39	2.09	5.56	0.44	28.74	0.07	0.23	0.35	-
BL5/21	333	*n*-C_{29}	0.99	0.49	0.19	1.88	9.47	0.36	28.88	0.25	0.03	N.D	-
BL5/22	342	*n*-C_{21}	1.59	0.48	1.40	1.19	0.88	0.63	27.71	0.29	0.19	N.D	-
BL5/24	365	*n*-C_{27}	1.17	0.50	0.47	1.92	3.14	0.47	28.86	0.49	0.10	N.D	-
BL5/26	386	*n*-C_{22}	0.87	0.57	0.42	1.63	5.42	0.54	28.35	0.18	0.06	0.13	-
BL5/28	409	*n*-C_{31}	0.96	0.53	0.44	1.45	4.71	0.47	28.57	0.21	0.02	0.01	-
BL5/31	441	*n*-C_{25}	1.16	0.49	0.57	1.62	3.25	0.55	28.14	0.15	0.23	0.18	+ [i]
BL5/33	460	*n*-C_{22}	1.00	0.54	0.66	1.44	3.18	0.59	28.18	0.21	0.29	0.35	++ [j]
BL5/34	464	*n*-C_{22}	0.72	0.54	0.63	1.59	2.98	0.51	28.68	0.34	0.02	0.24	+
BL5/35	473	*n*-C_{21}	0.79	0.53	0.73	1.51	2.62	0.54	28.35	0.21	0.28	0.44	+
BL5/36	488	*n*-C_{22}	0.75	0.55	0.80	1.40	2.01	0.49	28.75	0.42	0.02	0.21	++
BL5/38	507	*n*-C_{22}	0.68	0.56	0.53	1.09	4.17	0.41	28.98	0.27	0.03	N.D	++
minimum		/	0.68	0.45	0.15	1.09	0.88	0.33	27.71	0.07	0.02	0.01	/
maximum		/	2.03	0.57	1.40	2.19	11.16	0.63	28.98	0.49	0.29	0.44	/
average		/	1.13	0.51	0.50	1.68	5.11	0.49	28.52	0.26	0.11	0.19	/

*C_{max}=*n*-alkane maximum; [a] AI=alkane index=*n*-C_{31}/(*n*-C_{31}+*n*-C_{29}); [b] CPI=carbon preference index is determined by using the equation of Bray and Evans for full amplitude of *n*-alkanes (Tissot & Welte 1984); [c] TAR=terrigenous/aquatic ratio=(*n*-C_{27}+*n*-C_{29}+*n*-C_{31})/(*n*-C_{15}+*n*-C_{17}+*n*-C_{19}); [d] P_{aq}=aquatic macrophytes proxy=(*n*-C_{23}+*n*-C_{25})/(*n*-C_{23}+*n*-C_{25}+*n*-C_{29}+*n*-C_{31}); [e] ACL=average chain length=(25×*n*-C_{25}+27×*n*-C_{27}+29×*n*-C_{29}+31×*n*-C_{31}+33×*n*-C_{33})/(*n*-C_{25}+*n*-C_{27}+*n*-C_{29}+*n*-C_{31}+*n*-C_{33}); [f] Pr/Ph=pristane/phytane; ***i*-C_{25}=C_{25} regular isoprenoid; ***i*-C_{30}=C_{30} irregular isoprenoid (squalane); [g] N.D=Not Determined; [h] β-carotane was not detected; [i]+low abundance of β-carotane; [j]++high abundance of β-carotane.

BL5/13, BL5/15, and BL5/20 contain Type-II kerogen, and therefore high S2 and HI contents (up to 24.42 mg HC/g rock and 540 mg HC/g TOC, respectively), indicating algal biomass participation in the OM and/or terrigenous plant-derived hydrogen-rich OM (e.g., resins).

Judging by the average values of the C/N ratio for sediments of BL3 and BL5 (15.45 and 15.93, respectively, Table 2, El. Suppl. 3), it appears that mixed vascular and nonvascular plants characterize the OM (Meyers & Ishiwatari 1993). However, the values of the C/N ratio for most of the Prebreza sediments are near or over 20, suggesting somewhat greater participation of vascular plants. Surprisingly higher values of the C/N ratio (near or over 20) for most of the sediments enriched in Type II kerogen (Fig. 6a,b, El. Suppl. 3) probably relate to the occurrence of terrigenous plant-derived hydrogen-rich OM (Lüniger & Schwark 2002). This fact agrees with a general predominance of long-chain *n*-alkanes, indicated by the C_{max} (mostly at *n*-C_{27}, *n*-C_{29}, and *n*-C_{31}), CPI (up to 4.08 and 2.19 for BL3 and BL5, respectivley), *n*-C_{17}–*n*-C_{21}/*n*-C_{27}–*n*-C_{31} (under 1), and TAR (over 1) (Table 3; Tissot & Welte 1984; Bush & McInerney 2013). In contrast, sediments BL3/6, BL3/25, BL3/34, BL3/38, and BL3/40 indicate a substantial

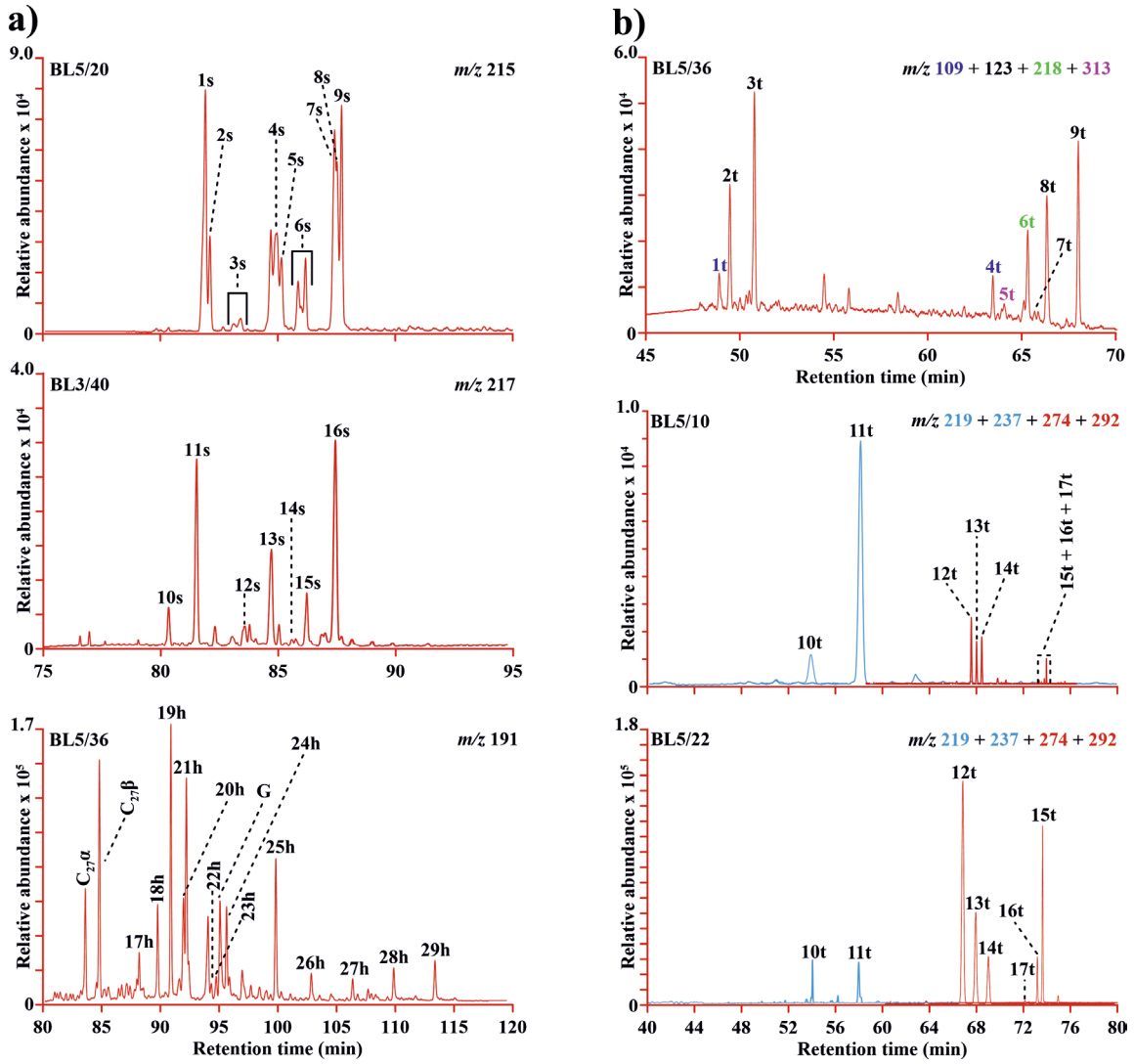

Fig. 5. a — Fragmentograms of sterenes (*m/z* 215), steranes (*m/z* 217), and terpanes (*m/z* 191) of representative samples BL5/20, BL3/40, and BL5/36, respectively. **b** — Saturated (*m/z* 109, 123, 218, and 313) and aromatic (*m/z* 178, 202, 219, 221, 223, 228, 233, 237, 241, 252, 274, and 292) di- and triterpenoids, along with unsubstituted PAHs of representative samples BL5/36, BL5/10, BL5/22, and BL5/35, respectively (the identification of peaks is given in Table 4).

presence of mid-chain *n*-alkanes, particularly *n*-C_{25} (Table 3, Fig. 4). In this context, the P_{aq} proxy displays values mostly over 0.50 (Table 3), meaning that submerged/floating macrophytes significantly contributed to the OM (Ficken et al. 2000). Interestingly, a higher participation of short-chain *n*-alkanes, thus algal/bacterial biomass, characterizes Prebreza sediments located below 333 m of the BL5, in which increasing values of the *n*-C_{17}–*n*-C_{21}/*n*-C_{27}–*n*-C_{31} ratio (up to 1.40), the C_{max} at *n*-C_{21} or *n*-C_{22}, as well as the presence of β-carotane, are observed (Table 3). On the other hand, only the sample BL3/10 (C-1) indicates somewhat greater participation of algal biomass (HI over 300 mg HC/g TOC, lower values of CPI and TAR parameters, along with the higher value of the *n*-C_{17}–*n*-C_{21}/*n*-C_{27}–*n*-C_{31} ratio, Tables 2, 3). Tree leaves and reed plants are also contributing to the OM, given that the *n*-C_{27} or *n*-C_{29} generally predominate over *n*-C_{31}, and values of the ACL parameter average about 28.40 for both studied boreholes (Table 3; Duan & He 2011).

In general, the S/H ratio shows a clear increasing trend of terrigenous and/or microbiologically reworked OM (S/H under 1) towards the upper section of the Prebreza unit of BL3 and BL5 (above 305 and 288 m, respectively, Table 5, Fig. 7a,d; Jiamo et al. 1990). This may indicate a gradual transition towards a freshwater lacustrine environment. This fact agrees with a general predominance of C_{29} over C_{27} steroids in the upper section of BL3 and BL5, which usually relates to vascular plants (Table 5; Schwark & Empt 2006). Some fluctuations of the S/H parameter in lithofacies A and B of the BL3 may relate to the presence of the resuspended OM, resulting from the river transport of eroded older sedimentary beds (Figs. 1c, 7a,d). Therefore, the sediments of these lithofacies potentially reflect a complex mixture of information on

Table 4: Identification of peaks of sterenes (*m/z* 215), steranes (*m/z* 217), terpanes (*m/z* 191) saturated and aromatic di- and triterpenoids, along with PAHs (*m/z* 109, 123, 178, 202, 218, 219, 221, 223, 228, 233, 237, 241, 252, 274, 292, and 313), Fig. 5a, b, respectively.

Peak	Compounds	Peak	Compounds
1s	C_{27} ($\Delta^4 + \Delta^2$)-sterenes	1t	Fitchelite
2s	C_{27} (Δ^5)-sterene	2t	Isopimarane
3s	C_{28}-steradienes	3t	ent-16β-kaurane
4s	C_{28} ($\Delta^4 + \Delta^2$)-sterenes	4t	*Des*-A-olean-13(18)-ene
5s	C_{28} (Δ^5)-sterene	5t	*Des*-A-urs-13(18)-ene
6s	C_{29}-steradienes	6t	*Des*-A-olean-12-ene
7s	C_{29} (Δ^4)-sterene	7t	*Des*-A-lup-5(10)-ene
8s	C_{29} (Δ^2)-sterene	8t	*Des*-A-lupane
9s	C_{29} (Δ^5)-sterene	9t	*Des*-A-oleanane/ursane
10s	C_{27} 5β(H), 14α(H), 17α(H)-20R sterane	10t	19-norabieta-8, 11, 13-ene
11s	C_{27} 5α(H), 14α(H), 17α(H)-20R sterane	11t	3,4-Dihydroretene
12s	C_{28} 5β(H), 14α(H), 17α(H)-20R sterane	12t	18-norabieta-8, 11, 13-ene
13s	C_{28} 5α(H), 14α(H), 17α(H)-20R sterane	13t	Tetrahydroretene
14s	C_{29} 5α(H), 14α(H), 17α(H)-20S sterane	14t	Simonellite
15s	C_{29} 5β(H), 14α(H), 17α(H)-20R sterane	15t	Retene
16s	C_{29} 5α(H), 14α(H), 17α(H)-20R sterane	16t	9-Methylretene
27α	17α(H)-22,29,30-trisnorhopane, Tm, C_{27} hopane		
27β	17β(H)-22,29,30-trisnorhopane, C_{27} hopane	17t	2-Methylretene
17h	17α(H), 21β(H)-norhopane, C_{29} hopane		
18h	17β(H), 21α(H)-normoretane, C_{29} moretane	18t	*Des*-A-dinoroleana-5, 7, 9, 11, 13-pentaene
19h	17α(H), 21β(H)-hopane, C_{30} hopane	19t	*Des*-A-dinorursa-5, 7, 9, 11, 13-pentaene
20h	17β(H), 21β(H)-hopane, C_{29} hopane	20t	*Des*-A-dinorlupa-5, 7, 9, 11, 13-pentaene
21h	17β(H), 21α(H)-moretane, C_{30} moretane	21t	*Des*-A-trinoroleana-5, 7, 9, 11, 13, 15, 17-heptaene
22h	17α(H), 21β(H)-22S-homohopane, C_{31} homohopane	22t	*Des*-A-trinorursa-5, 7, 9, 11, 13, 15, 17-heptaene
23h	17α(H), 21β(H)-22R-homohopane, C_{31} homohopane	23t	*Des*-A-trinorlupa-5, 7, 9, 11, 13, 15, 17-heptaene
G	Gammacerane	24p	Phenanthrene
24h	17β(H), 21β(H)-hopane, C_{30} hopane	25p	Fluoranthene
25h	17β(H), 21α(H)-22R-moretane, C_{31} moretane	26p	Pyrene
26h	17β(H), 21α(H)-22R-moretane, C_{32} moretane	27p	Benz[*a*]anthracene
27h	17β(H), 21α(H)-22R-moretane, C_{33} moretane	28p	Benzo[*e*]pyrene
28h	17β(H), 21α(H)-22R-moretane, C_{34} moretane	29p	Benzo[*a*]pyrene
29h	17β(H), 21α(H)-22R-moretane, C_{35} moretane	30p	Perylene

paleoclimatic and paleoenvironmental conditions from different older and younger depositional cycles.

Maturity of the OM

The T_{max} suggests that the OM is between the immature (under 435 °C) and early mature stages (between 435 and 445 °C, Table 2; Peters 1986). However, due to possible interactions of the OM and mineral matrix, along with low amounts of S2 (under 0.2 mg HC/g rock, Table 2) for various samples, the results seem questionable, meaning that they do not accurately represent the thermal evolution of the OM (Peters 1986). Reliable T_{max} values for samples with higher S2 contents (over 0.20 mg HC/g rock, Table 2) suggest that maturity ranges between immature and early mature stages, indicating the beginning of the oil window (Fig. 6b).

Nevertheless, highly abundant $\Delta^{2, 4, 5}$ sterenes, C_{30} βα moretane, and C_{31} 17β, 21α(H)-22R moretane, along with low C_{31} homohopane ratio and low C_{29} sterane ratio indicate that the OM is thermally immature (Table 5, Fig. 5a; Seifert & Moldowan 1980; Larcher et al. 1987; Peters & Moldowan 1991). Compared to others, the C_{31} homohopane ratio has displayed some variations in maturity for samples BL3/39 and BL5/33, and the values are somewhat elevated, suggesting the higher thermal evolution of the OM. However, the values of these parameters have not reached the thermodynamic equilibrium for oil generation (Seifert & Moldowan 1980; Peters & Moldowan 1991).

Depositional environment

Coarser sediments found in the BL3 Prebreza formation suggest a more dynamic depositional environment. It seems that alluvial processes influenced to a greater extent the sedimentary deposition in the part of the basin where BL3 is located (see the section Geological settings, Table 1, Figs. 1c, 2). Given that fact, high sedimentation rates are probably responsible for preserving the OM in the Prebreza sediments of lithofacies C-1, which is a zone of higher TOC (up to 6.64 wt. %, Table 2; Schulte et al. 2000). Only the sample BL3/6 (C-1) has displayed the lowest TOC content, which

Table 5: The results of specific organic geochemical parameters of studied samples, calculated from the distribution and relative abundance of steroids and terpenoids.

Sample	Depth (m)	S/H [a]	%C_{27} or %ΔC_{27} [b]	%C_{28} or %ΔC_{28} [c]	%C_{29} or %ΔC_{29} [d]	$C_{30}M/C_{30}H$ [e]	C_{31} (22S)/(22S+22R) [f]	C_{29} (20S)/(20S+20R) [g]	GI [h]
BL3/5 *	113	0.33	15.38	17.88	66.74	N.D [i]	N.D	N.D	8.64
BL3/6	127	0.19	29.44	38.56	32.00	0.55	0.29	0.09	3.64
BL3/8	148	3.89	63.55	12.68	23.77	8.50	N.D	N.D	8.29
BL3/9	165	2.55	51.31	13.48	35.21	4.52	0.21	0.07	4.40
BL3/10	190	0.47	35.12	34.57	30.31	0.54	0.43	0.09	3.39
BL3/11	207	0.33	26.90	31.55	41.55	0.50	0.45	0.12	4.47
BL3/16	305	0.19	25.63	36.97	37.40	1.08	0.42	N.D	4.61
BL3/25	465	2.40	23.12	18.20	58.68	1.36	0.30	N.D	6.38
BL3/34	567	0.48	24.10	23.88	52.02	0.68	0.30	0.10	6.56
BL3/38	602	2.21	50.36	20.16	29.48	3.82	0.16	N.D	7.62
BL3/39	611	13.30	19.32	17.05	63.64	0.80	0.46	0.01	4.78
BL3/40	637	2.70	34.77	23.69	41.54	0.84	0.41	0.04	6.36
minimum		0.19	15.38	12.68	23.77	0.50	0.16	0.01	3.39
maximum		13.30	63.55	38.56	66.74	8.50	0.46	0.12	8.64
Sample	**Depth (m)**	**S/H**	**%C_{27} or %ΔC_{27}**	**%C_{28} or %ΔC_{28}**	**%C_{29} or %ΔC_{29}**	**M/H**	**C_{31} (22S)/(22S+22R)**	**C_{29} (20S)/(20S+20R)**	**GI**
BL5/10	209	0.21	23.14	17.75	59.11	0.60	0.16	N.D	6.79
BL5/13	245	0.18	24.89	15.11	60.00	0.60	0.05	N.D	8.51
BL5/15	260	0.69	34.67	6.50	58.82	3.91	0.06	N.D	8.39
BL5/16	277	0.24	33.80	29.16	37.04	0.75	0.28	0.07	5.01
BL5/17	288	5.17	17.69	54.23	28.08	2.28	0.30	N.D	6.39
BL5/19	305	3.05	39.05	28.03	32.92	1.53	0.32	N.D	4.33
BL5/20	319	1.94	33.75	14.11	52.14	3.63	0.19	N.D	4.52
BL5/21	333	3.09	51.90	24.46	23.64	1.68	0.21	N.D	5.62
BL5/22	342	1.50	61.76	29.52	8.72	1.97	0.40	N.D	2.72
BL5/24	365	2.22	24.47	24.89	50.64	0.89	0.43	N.D	3.72
BL5/26	386	3.31	27.28	40.26	32.46	2.20	0.39	0.04	2.91
BL5/28	409	1.12	40.58	18.91	40.51	0.57	0.45	N.D	3.91
BL5/31	441	7.18	36.35	29.33	34.32	2.86	0.36	0.01	5.01
BL5/33	460	10.12	17.60	37.48	44.92	2.78	0.48	0.01	2.32
BL5/34	464	1.94	28.22	36.91	34.88	0.80	0.45	0.05	2.66
BL5/35	473	4.71	13.20	10.88	75.92	1.30	0.43	0.02	4.59
BL5/36	488	4.27	31.02	32.43	36.55	0.70	0.40	0.03	2.35
BL5/38	507	12.40	30.23	27.43	42.34	0.28	0.32	0.03	2.07
minimum		0.18	13.20	6.50	8.72	0.28	0.05	0.01	2.07
maximum		12.40	51.90	54.23	75.92	3.91	0.48	0.07	8.51

***Highly abundant sterene isomers characterize bolded samples;** [a] S/H=∑Steroids/∑Hopanoids=$\sum C_{27-29}$ ααα(S+R)-steranes or $\sum C_{27-29}(\Delta^2+\Delta^4+\Delta^5)$-sterenes/$\sum C_{29-33}$ αβH-hopanes; [b] %C_{27}=100×C_{27} ααα20(R)-sterane/$\sum(C_{27}$ ααα20(R)+C_{28} ααα20(R)+C_{29} ααα20(R))-steranes or %ΔC_{27}=100×C_{27} $(\Delta^2+\Delta^4+\Delta^5)$-sterenes/$\sum(C_{27}$ $(\Delta^2+\Delta^4+\Delta^5)$+$C_{28}(\Delta^2+\Delta^4+\Delta^5)$+$C_{29}(\Delta^2+\Delta^4+\Delta^5)$)-sterenes; [c] %$C_{28}$=100×$C_{28}$ ααα20(R)-sterane/$\sum(C_{27}$ ααα20(R)+C_{28} ααα20(R)+C_{29} ααα20(R))-steranes or %ΔC_{28}=100×$C_{28}(\Delta^2+\Delta^4+\Delta^5)$-sterenes/$\sum(C_{27}(\Delta^2+\Delta^4+\Delta^5)$+$C_{28}(\Delta^2+\Delta^4+\Delta^5)$+$C_{29}(\Delta^2+\Delta^4+\Delta^5)$)-sterenes; [d] %$C_{29}$=100×$C_{29}$ααα20(R)-sterane/$\sum(C_{27}$ααα20(R)+$C_{28}$ ααα20(R)+C_{29} ααα20(R))-steranes or %ΔC_{29}=100×$C_{29}(\Delta^2+\Delta^4+\Delta^5)$-sterenes/$\sum(C_{27}(\Delta^2+\Delta^4+\Delta^5)$+$C_{28}(\Delta^2+\Delta^4+\Delta^5)$+$C_{29}(\Delta^2+\Delta^4+\Delta^5)$)-sterenes; [e] $C_{30}M/C_{30}H$=moretane/hopane=C_{30} moretane/C_{30} hopane; [f] C_{31} (22S)/(22S+22R)=C_{31} homohopane (22S)/(22S+22R); [g] C_{29} (20S)/(20S+20R)=C_{29} sterane ααα20(S)/C_{29} sterane ααα20(S)+C_{29} sterane ααα20(R); [h] GI (Gammacerane index)=10×Gammacerane/(Gammacerane+C_{30}-hopane); [i] N.D=Not Determined.

probably relates to paleoredox (slightly oxic conditions) or paleoclimate (dry and arid periods) conditions. On the other hand, significant portions of major elements that assemble clay minerals have resulted from alluvial or lacustrine shallowing processes, diluting and reducing OM contents (TOC under 0.60 wt. % Tables 1, 2).

The preservation of the OM in the studied basin area may also be related to oxygen-depleted, alkaline, and saline zones, which are marked by relatively high contents of Fe_2O_3, or highly abundant phytane, *i*-C_{25}, and *i*-C_{30} (Tables 1, 3; Didyk et al. 1978; Sinninghe Damasté et al. 1995). Higher alkalinity and salinity (*i*-C_{25}/*n*-C_{22} and *i*-C_{30}/*n*-C_{26} up to 0.29 and 0.44, C/S mostly under 10, Tables 2, 3; Berner & Raiswell 1984; Leventhal 1987), along with the anoxic conditions (Pr/Ph<1, Table 3), appears to be a more decisive factor for preserving the OM in the sediments of the BL5. Given that the occurrence of β-carotane characterizes sediments deposited under 333 m, may suggest the saline lacustrine environment (Table 3, Fig. 4; Jiang & Fowler 1986). On the other hand, the OM preservation in the BL3 may relate to either dysoxic conditions or high sedimentation rates (Schulte et al. 2000).

Additionally, highly abundant gammacerane probably results from the stratified water column caused by temperature gradients rather than hypersalinity since there is no evidence of it in the investigated sediments (Collister et al. 1992; Sinninghe Damasté et al. 1995).

Table 6: The results of specific organic geochemical parameters of studied samples, calculated from the distribution and relative abundance of saturated and aromatic terpenoids, as well as unsubstituted PAHs.

Sample	Lithofacies	Depth (m)	al-AGR *[a]	∑Saturated tri-/ ∑Aromatic triterpenoids	ar-AGR *[b]	ar-AGR$_{ole}$ [c]	al, ar-AGR [d]	LMW$_{PAHs\ (unsubstituted)}$/ HMW$_{PAHs\ (unsubstituted)}$ [e, f]
BL3/5	C-1	113	0.03	4.67	0.05	0.94	0.03	1.44
BL3/6		127	0.24	N.D [g]	1.00	0.00	0.87	5.63
BL3/8		148	0.70	0.26	0.27	0.68	0.43	6.13
BL3/9		165	0.21	2.11	0.16	0.81	0.20	6.47
BL3/10		190	0.44	1.98	0.24	0.70	0.38	0.10
BL3/11	B	207	0.22	3.82	0.37	0.54	0.26	0.26
BL3/16	A	305	0.37	0.09	0.13	0.83	0.16	0.18
BL3/25		465	0.85	0.02	0.25	0.69	0.30	2.19
BL3/34		567	0.50	0.33	0.20	0.75	0.31	1.23
BL3/38	C-2	602	0.71	0.34	0.20	0.75	0.44	1.52
BL3/39		611	0.29	0.23	0.05	0.94	0.11	2.77
BL3/40		637	0.37	0.67	0.13	0.83	0.24	4.41
minimum			0.03	0.02	0.05	0.00	0.03	0.10
maximum			0.85	4.67	1.00	0.94	0.87	6.47
average			0.41	1.32	0.25	0.71	0.31	2.69
Sample	**Lithofacies**	**Depth (m)**	**al-AGR**	**∑Saturated tri-/ ∑Aromatic triterpenoids**	**ar-AGR**	**ar-AGR$_{ole}$**	**al, ar-AGR**	**LMW$_{PAHs\ (unsubstituted)}$/ HMW$_{PAHs\ (unsubstituted)}$**
BL5/10	Swamp	209	0.23	0.54	0.78	0.13	0.70	0.23
BL5/13		245	0.27	0.69	0.51	0.43	0.44	8.63
BL5/15	Lacustrine	260	0.54	0.16	0.29	0.68	0.34	1.11
BL5/16		277	0.57	0.14	0.31	0.60	0.35	0.96
BL5/17		288	0.34	0.22	0.14	0.82	0.18	0.44
BL5/19		305	0.71	0.06	0.09	0.88	0.19	3.90
BL5/20		319	0.65	0.07	0.22	0.74	0.27	11.51
BL5/21		333	0.55	0.02	0.11	0.86	0.13	4.51
BL5/22		342	0.70	0.01	0.17	0.77	0.18	0.28
BL5/24		365	1.00	N.D	0.33	0.62	0.48	7.73
BL5/26		386	0.63	0.02	0.29	0.66	0.30	4.30
BL5/28		409	0.80	0.01	0.52	0.42	0.52	4.29
BL5/31		441	0.64	0.05	0.12	0.84	0.17	2.88
BL5/33		460	0.52	0.16	0.23	0.72	0.29	0.75
BL5/34		464	0.57	0.02	0.05	0.93	0.08	0.82
BL5/35		473	0.74	0.01	0.12	0.86	0.14	1.08
BL5/36		488	0.54	0.08	0.10	0.87	0.16	0.39
BL5/38		507	0.33	0.10	0.05	0.92	0.09	0.18
minimum			0.23	0.01	0.05	0.13	0.08	0.18
maximum			1.00	0.69	0.78	0.93	0.70	11.51
average			0.57	0.14	0.25	0.71	0.28	3.00

* Table 4 has presented saturated and aromatic terpenoids that are used for the calculation of terpenoid parameters; [a] al-AGR=∑saturated diterpenoids/(∑saturated diterpenoids+∑saturated triterpenoids); [b] ar-AGR=∑aromatic diterpenoids/(∑aromatic diterpenoids+∑aromatic triterpenoids); [c] ar-AGRole=∑aromatic triterpenoids with an oleanane carbon skeleton/(∑aromatic diterpenoids+∑aromatic triterpenoids with an oleanane carbon skeleton); [d] al, ar-AGR+∑aromatic and saturated diterpenoids/(∑aromatic and saturated diterpenoids+∑aromatic and saturated triterpenoids); [e] Low molecular weight unsubstituted PAHs (LMW_{PAHs}) are phenanthrene, fluoranthene, pyrene, benz[*a*]anthracene, while benzo[*e*]pyrene, benzo[*a*]pyrene, and perylene are high molecular weight unsubstituted PAHs (HMW_{PAHs}); [f] $LMW_{PAHs\ (unsubstituted)}/HMW_{PAHs\ (unsubstituted)}$=(phenanthrene+fluoranthene+pyrene+benz[*a*]anthracene)/(benzo[*e*]pyrene+benzo[*a*]pyrene+perylene); [g] N.D=Not Determined.

Paleoclimate and paleovegetation interpretation

Fu et al. (2015), Liu & Zhou (2007), and Xie et al. (2018) have proposed a few widely applied inorganic paleoclimate indicators, such as C-value, Sr/Cu, and Rb/Sr ratio (Fig. 3a–f). The study of Fu et al. (2015) has proposed boundaries of the C-value for arid (0–0.20), semi-arid (0.20–0.40), semi-arid/semi-humid (0.40–0.60), semi-humid (0.60–0.80), and humid (0.80–1) conditions (Fig. 3). On the other hand, the investigations of Liu & Zhou (2007) and Xie et al. (2018) have indicated that the sedimentation under warm and humid climatic conditions is marked by low Sr/Cu (under 10) and high Rb/Sr, while the opposite suggests cold and arid climate conditions (Fig. 3). The results indicating that the deposition of Čučale sediments in the BL3 (lithofacies C-2 and A-the sample BL3/34) characterizes warm and semi-humid/semi-arid to semi-humid climate periods (C-value between 0.53 and 0.67, Sr/Cu under 10, and Rb/Sr up to 0.52, Table 1, Fig. 3a–c; Fu et al. 2015; Liu & Zhou 2007; Xie et al. 2018). The sedimentation of the Prebreza sediments (BL3 borehole-lithofacies A-excluding BL3/34) progressed under similar climatic conditions (Table 1, Fig. 3a–c). As the deposition of the Prebreza sediments continued, climate conditions shifted from warm and semi-humid/semi-arid towards more cold and arid

periods, particularly at two depth intervals, from 305 to 207 m and 148 to 127 m (C-value under 0.20, Sr/Cu over 35, and Rb/Sr under 0.04, Table 1, Fig. 3a–c; Fu et al. 2015; Liu & Zhou 2007; Xie et al. 2018). Nevertheless, at depth intervals, from 190 to 165 m and 127 to 113 m, the climate transitions back towards warm and semi-arid/semi-humid periods (C-value over 0.52, Sr/Cu around 5, and Rb/Sr under 0.27, Table 1, Fig. 3a–c; Fu et al. 2015; Liu & Zhou 2007; Xie et al. 2018). On the other hand, warm and semi-humid/semi-arid climate conditions have mostly characterized the depositional period of the Prebreza sediments of the BL5, with some cold and arid intervals, particularly at 319 m (BL5/20), 342 m (BL5/22), and 473 m (BL5/35) in the lacustrine unit (C-value under 0.20, Sr/Cu over 21, and Rb/Sr under 0.06, Table 1, Fig. 3d–f; Fu et al. 2015; Liu & Zhou 2007; Xie et al. 2018).

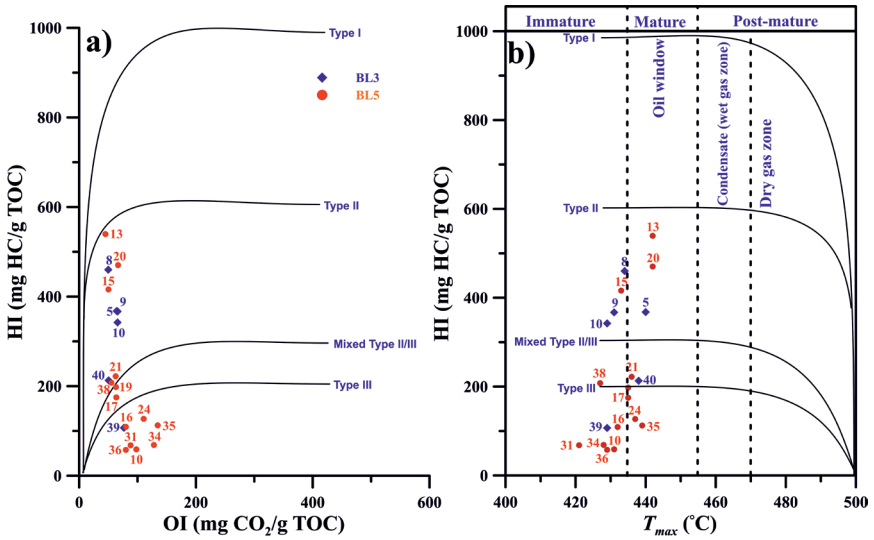

Fig. 6. Cross-plots of (**a**) HI vs. OI and (**b**) HI vs. T_{max}, indicating kerogen type and maturity (Peters 1986; Peters et al. 2005). Čučale Fm.: BL3/39 and BL3/40; Prebreza Fm.: BL3/5–10, BL5/10–38. The graphs show only reliable values, selected according to Peters' criteria (Peters 1986). See the text for more information.

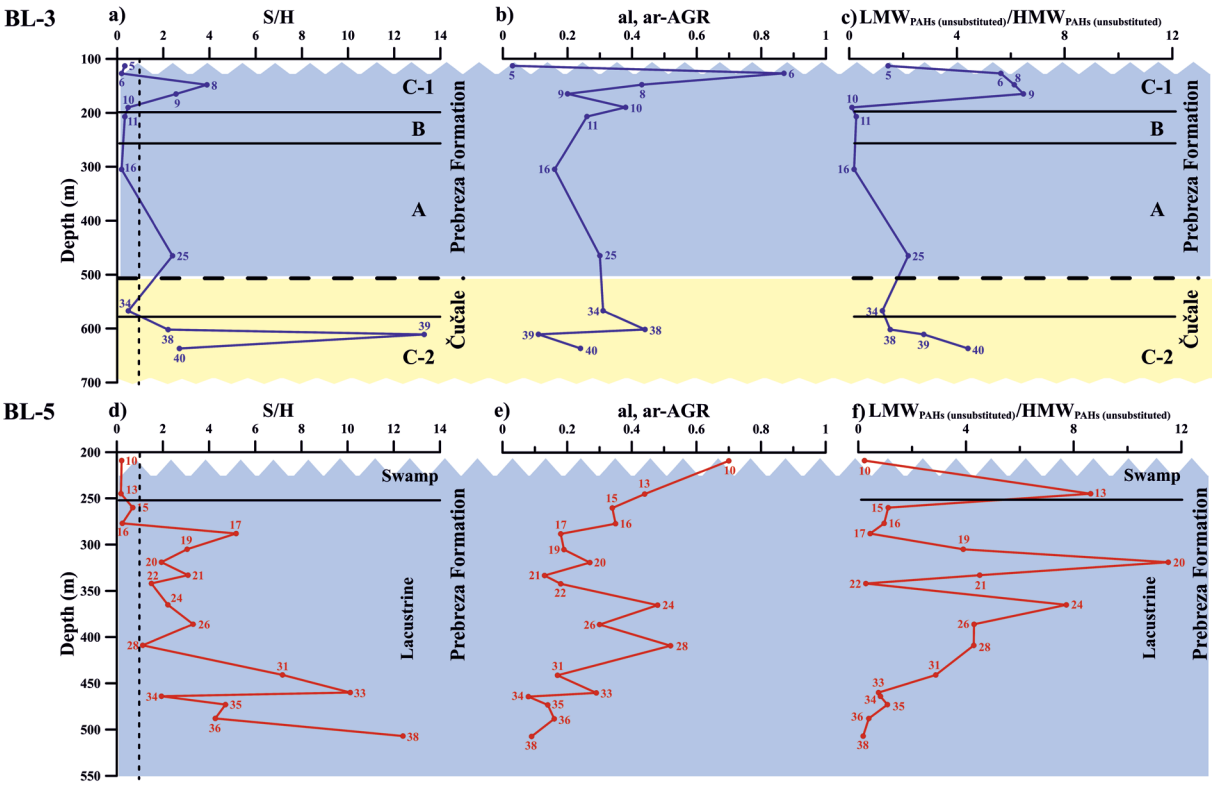

Fig. 7. The S/H ratio (OM with S/H<1 microbially reworked /terrestrial origin, S/H>1 algal origin, Jiamo et al. 1990), al, ar-AGR, and $LMW_{PAHs\ unsubstituted}/HMW_{PAHs\ unsubstituted}$ for sediments of the BL3 (**a–c**) and BL5 (**d–f**).

Some studies have suggested the application of vascular di- and triterpenoids and PAHs as a valuable tool for tracing paleoflora and paleoclimatic changes since their presence may be related to seasonality, temperature, and humidity variations (Soma et al. 1996; Hautevelle et al. 2006; Xu et al. 2019). Diterpenoids with an abietane, isopimarane, or kaurane carbon skeleton mostly originate from resins and waxes of coniferous gymnosperms (Otto & Wilde 2001; Hautevelle et al. 2006). The precursors of *des*-A-triterpenoids are α- and β-amyrin, occurring in the root, wood, and bark of most angiosperms (Bechtel et al. 2003; Huang et al. 2013). PAHs may arise through both diagenetic/catagenetic transformations and combustion processes of vascular plants that originate from gymno- or angiosperm plant taxa (Xu et al. 2019). In this case, the changes in paleoclimate conditions are tracked with several parameters that are based on the distribution and relative abundance of these compounds (Fig. 5b). However, the occurrence of gymno- and angiosperms within almost all climate zones complicates the interpretation of the parameters, and therefore this study recommends comparing the inorganic with organic paleoclimate parameters (Hautevelle et al. 2006; Zhang et al. 2018).

Nevertheless, difficulty in applying these parameters is encountered. Kalkreuth et al. (1998) and Nakamura et al. (2010) have pointed out that the aliphatic triterpenoids are more easily altered to aromatic derivatives during diagenesis, meaning that some terpenoid parameters may not accurately display vegetational changes. Several factors, such as redox conditions, clay-catalysed processes, or microbial activity, may promote the aromatization mechanism. The ∑Saturated tri-/∑Aromatic triterpenoids parameter suggests that the progressive aromatization of saturated to aromatic triterpenoid derivatives has occurred in the BL5 (under 1, Table 6). The process is somehow prevented for most of the samples in the lithofacies B and C-1 of the BL3 (over 1, Table 6). Therefore, a higher presence of saturated diterpenoids corroborates a weaker influence of alluvial processes, suggesting that minor occurrence of clay mineral representatives/microorganisms that could catalyse the aromatization or high sedimentation rates have probably hindered the process in these lithofacies (Tables 1, 6, Fig. 2). For this reason, the study considers the parameter based on the distribution and relative abundance of both saturated and aromatic terpenoids (al, ar-AGR, Table 6, Fig. 7b, e).

Previous research by Černjavski (1932) has provided the postglacial paleoflora characterization of the Toplica Basin, suggesting *Betulaceae*, *Fagaceae*, *Malvaceae*, *Pinaceae*, *Salicaceae*, *Typhaceae,* and *Ulmaceae* as prevalent plant families representing the northern Balkan province. Interestingly, the occurrence of these plant families in the Toplica Basin is also in agreement with recent studies of the Middle Miocene paleoflora in Serbia, which was a part of the former Central Paratethys region (Utescher et al. 2007a,b; Ivanov et al. 2011). Based on inorganic paleoclimate proxies, as well as paleoflora and stratigraphy data, the parameters should reflect which plant family becomes more or less dominant in the depth zones where the most significant climate change is observed (Tables 1, 6, Figs. 2, 3). For instance, warm and semi-humid/semi-arid to semi-humid climate conditions characterize the depositional period of Lower to Middle Miocene Čučale and Prebreza sediments in lithofacies C-2 and A of the BL3 (Tables 1, Figs. 2, 3a–c), in which angiosperm remains predominate (ar-AGR and al, ar-AGR under 0.50, Table 6, Fig. 7b). Investigations of Kováč et al. (2007), Piller et al. (2007), Utescher et al. (2007a,b), and Ivanov et al. (2011) have documented mixed angio-/gymnosperms elements in the Lower Miocene, and the predominance of angiosperms during Middle Miocene of the Central Paratethys, especially throughout the Badenian, pointing out warm and humid climatic phase, and reflecting the Middle Miocene Climate Optimum (MMCO). According to Ivanov et al. (2011) and Utescher et al. (2007a,b), mixed mesophytic forests, especially laurophyllous elements with some deciduous taxa, mostly made up the vegetation of Lower and Middle Miocene in Serbia. Additionally, a general prevalence of LMW over HMW PAHs ($LWM_{PAHs\ (unsubstituted)}/HMW_{PAHs\ (unsubstituted)}$ over 1, Table 6, Fig. 7c) in these sediments suggests that their production relates mainly to paleo-wildfires, resulting from volcanic activity (Miocene Lece volcanics, see the section Geological settings) or lightning strikes (Fabiańska & Kurkiewicz 2013; Abarzúa et al. 2016).

The cold and arid climate periods have characterized sedimentary deposition in lithofacies B and C-1 of the BL3 (Table 1, Fig. 3a–c), together with increasing portions of gymnosperm remnants, which reach their maximum for the sample BL3/6 (al, ar-AGR up to 0.87, Table 6, Fig. 7b). The study by Ivanov et al. (2011) mentions the presence of certain coniferous elements, such as *Pinaceae*, which species may adapt to dry environments (Hautevelle et al. 2006). As suggested by Kováč et al. (2007), Jiménez-Moreno et al. (2008), and Utescher et al. 2007b during the Middle Miocene, a climatic cooling occurred in basins of the Central Paratethys, especially during the Late Badenian/Sarmatian and at the end of Early Badenian. Additionally, the study by Randazzo et al. (1999) has pointed out that episodes of tectonism and volcanism during the Middle Miocene may account for the paleoclimate represented by the cool-water carbonate sediments of the Paratethys, which may also explain this climatic change in lithofacies B and C-1 (Table 1, see sections Geological settings and Major and trace elements). It is worth mentioning that the P_{aq} parameter reached a maximum in the lithofacies C-1, particularly for sample BL3/6 (Table 3), suggesting the presence of some well-adapted submerged/floating macrophytes under cooler climatic conditions (Ficken et al. 2000; Chambers et al. 2008). Nevertheless, it should be taken into account that fine-grained clastic material might have transported the OM rich in gymnosperm remains into the basin via alluvial flows, probably originating from higher mountainous areas characterized by cold/arid to semi-arid climate intervals (Tables 1, 6; Fig. 7b). Even though LMW PAHs mostly predominate in the Prebreza sediments of lithofacies B and C-1 ($LWM_{PAHs\ (unsubstituted)}/HMW_{PAHs\ (unsubstituted)}$ up to 6.47,

Table 6, Fig. 7c), higher portions of HMW PAHs, particularly perylene, in samples BL3/10 and BL3/11 are recorded ($LWM_{PAHs\ (unsubstituted)}/HMW_{PAHs\ (unsubstituted)}$ under 1, Table 6, Fig. 7c). According to Soma et al. (1996), Bechtel et al. (2007), and Xu et al. (2019), the accumulation and preservation of perylene relate mostly to either anoxic depositional conditions or specific precursor biomass, thereby suggesting its biogenic origin, which may be the case for these samples (see sections Type of OM and Depositional environment).

Furthermore, the deposition of lacustrine Prebreza sediments, as well as the transition point from lacustrine to swamp unit (BL5/13), in the borehole BL5 took place mostly under warm and semi-humid/humid climate conditions (Table 1, Fig. 3d–f). Surprisingly high values of the ar-AGR_{ole} parameter for samples BL5/20, BL5/22, and BL5/35 (up to 0.86, Table 6), from a depositional period with a cold and arid climate (Table 1, Fig. 3d–f), indicate the prevalence of angiosperms instead of gymnosperms. A possible explanation may be in the origin of retene. The study of Wen et al. (2000) has proposed that alternative sources of retene are algal and bacterial precursors. Since a significant contribution of steroids (S/H over 1, Fig. 6d) has marked these sediments (Tables 3, 5), it is highly probable that retene has an algal rather than terrestrial origin, meaning that terpenoid parameters cannot accurately reflect an actual contribution of gymnosperms. It may suggest that during the depositional period of these sediments a decrease in precipitation and supply of the OM derived by vascular plants transported via alluvial-lacustrine system into the basin has occurred. Another explanation would be the presence of xerophytic legume-like taxa reported in various studies (Utescher et al. 2007a,b; Ivanov et al. 2011). Higher values of C/N (>15) indicate the presence of terrigenous OM as well (Table 2).

Moreover, warm and semi-arid/semi-humid to humid climate conditions are also maintained in the swamp unit (Table 1, Fig. 3d–f), where coaly clay sediments are present, suggesting that coal-forming plants relate to the gymnosperms (ar-AGR and al, ar-AGR up to 0.78 and 0.70, Table 6, Fig. 7e). Utescher et al. (2007a,b) and Ivanov et al. (2011) have pointed out that gymnosperm representatives, namely *Sequoia*, *Cupressaceae*, and *Pinus*, are an important element of the Middle Miocene vegetation. A slightly higher contribution of HMW PAHs, especially perylene (Fig. 5b), characterizes sediments of the BL5 in comparison to BL3 ($LWM_{PAHs\ (unsubstituted)}/HMW_{PAHs\ (unsubstituted)}$ under 1, Table 6, Fig. 7f). Nevertheless, paleo-wildfires still seem to be the main cause for the production and accumulation of LMW PAHs in both swamp and lacustrine units, particularly for samples BL5/13 and BL5/20 ($LWM_{PAHs\ (unsubstituted)}/HMW_{PAHs\ (unsubstituted)}$ up to 8.63 and 11.51, respectively, Table 6, Fig. 7f).

Conclusion

This study focused on the influence of alluvial-lacustrine processes and paleoclimate variations on the distribution of vascular plant biomarkers and unsubstituted PAHs. Insight into the type and maturity of OM, as well as the depositional environment, were also presented.

Sandy silt and gravel components in the upper part of the BL3 suggest the presence of thicker clastites transported via alluvial flows, while fine-grained clastites characterize lower parts of the BL3, as well as lacustrine and swamp units of the BL5. Low TOC contents for various sediments in the BL3 and BL5 boreholes relate to either paleoredox/paleoclimate conditions or alluvial-lacustrine shallowing processes.

Generally, the results of T_{max}, HI, and C/N indicate that the studied sediments contain thermally immature to early mature mixed terrigenous and algal organic OM. A more pronounced presence of plant terpenoids and PAHs in the investigated sediments, which reflected paleoflora and paleoclimatic changes, relates to the presence of Type II, III, and II/III kerogens. The progressive aromatization of saturated to aromatic triterpenoid derivatives has occurred in the BL5 (low ∑Saturated tri-/∑Aromatic triterpenoids), whereas the process is somehow prevented for most of the samples in the lithofacies B and C-1 (BL3). The difference in the occurrence of microorganisms or intensity of alluvial processes between lithofacies of the BL3, or high sedimentation rates has probably hindered the aromatization process in lithofacies B/C-1. Warm and semi-humid/semi-arid to semi-humid climate periods, supported by high C-value and Rb/Sr with low Sr/Cu ratios, have mostly characterized the deposition of Lower/Middle Miocene Čučale and Prebreza sediments, reflecting the MMCO, with some cooling periods. Lower/Middle Miocene Prebreza and Čučale sediments are mostly characterized by angiosperm remnants, as indicated by elevated ar-AGR_{ole} and decreased al, ar-AGR parameters. The production of LMW PAHs in studied sediments relates to paleo-wildfires, probably caused by volcanic activity or lightning strikes, while the presence of HMW PAHs, particularly perylene, is associated with anoxic conditions or specific biomass precursor.

Acknowledgements: The Ministry of Education, Science and Technological Development of the Republic of Serbia (Grant No. 451-03-68/2021-14/200026 and 451-03-9/2021-14/200168, and Projects No. 176006 and 176019) financially supported this work. We are grateful to reviewers for useful comments and suggestions, especially to Dr. Júlia Kotulová, but also to Prof. Dr. Ljupko Rundić and Prof. Dr. Nebojša Vasić for providing sedimentological and stratigraphy data, which significantly improved this paper.

References

Abarzúa A.M., Vargas C., Jarpa L., Gutiérrez N.M., Hinojosa L.F. & Paula S. 2016: Evidence of Neogene wildfires in Central Chile: Charcoal records from the Navidad formation. *Palaeogeography, Palaeoclimatology, Palaeoecology* 459, 76–85. https://doi.org/10.1016/j.palaeo.2016.06.036

Bechtel A., Gruber W., Sachsenhofer R.F., Gratzer R. & Püttmann W. 2001: Organic geochemical and stable carbon isotopic investigation of coals formed in low-lying and raised mires within the Eastern Alps (Austria). *Organic Geochemistry* 32, 1289–1310. https://doi.org/10.1016/S0146-6380(01)00101-2

Bechtel A., Sachsenhofer R.F., Markic M., Gratzer R., Lücke A. & Püttmann W. 2003: Paleoenvironmental implications from biomarker and stable isotope investigations on the Pliocene Velenje lignite seam (Slovenia). *Organic Geochemistry* 34, 1277–1298. https://doi.org/10.1016/S0146-6380(03)00114-1

Bechtel A., Widera M., Sachsenhofer R.F., Gratzer R., Lücke A. & Woszczyk M. 2007: Biomarker and stable carbon isotope systematics of fossil wood from the second Lusatian lignite seam of the Lubstow deposit (Poland). *Organic Geochemistry* 38, 1850–1864. https://doi.org/10.1016/j.orggeochem.2007.06.018

Berner R.A. & Raiswell R. 1984: C/S method for distinguishing freshwater from marine sedimentary rocks. *Geology* 12, 365–368. https://doi.org/10.1130/0091-7613(1984)12<365:CMFDFF>2.0.CO;2

Burazer N., Šajnović A., Vasić N., Kašanin-Grubin M., Životić D., Mendonça-Filho J., Vulić P. & Jovančićević B. 2020: Influence of paleoenvironmental conditions on distribution and relative abundance of saturated and aromatic hydrocarbons in sediments from the NW part of the Toplica basin, Serbia. *Marine and Petroleum Geology* 115, 104252. https://doi.org/10.1016/j.marpetgeo.2020.104252

Bush R.T. & McInerney F.A. 2013: Leaf wax *n*-alkane distributions in and across modern plants: Implications for paleoecology and chemotaxonomy. *Geochimica et Cosmochimica Acta* 117, 161–179. https://doi.org/10.1016/j.gca.2013.04.016

Chambers P.A., Lacoul P., Murphy K.J. & Thomaz S.M. 2008: Global diversity of aquatic macrophytes in freshwater. *Hydrobiologia* 595, 9–26. https://doi.org/10.1007/s10750-007-9154-6

Černjavski P. 1932: Beitrag zur postglazialen Geschichte des Blace-"Sees" in Serbien. *Bulletin De L'institute Et Du Jardin Botaniques De L'université De Beograd* 2, 80–90.

Collister J.W., Summons R.E., Lichtfouse E. & Hayes J.M. 1992: An isotopic biogeochemical study of the Green River oil shale. *Organic Geochemistry* 19, 265–276. https://doi.org/10.1016/0146-6380(92)90042-V

Didyk B.M., Simoneit B.R.T., Brassell S.C. & Eglinton G. 1978: Organic geochemical indicators of paleoenvironmental conditions of sedimentation. *Nature* 272, 216–222. https://doi.org/10.1038/272216a0

Dragić D., Miskovic A., Hart C., Tosdal R., Fox P. & Glisic S. 2014: Spatial and temporal relations between epithermal and porphyry style mineralization in the Lece Magmatic Complex, Serbia. In: Proceedings of the SEG Conference "Building Exploration Capability for the 21st Century". *Society of Economic Geologists*, United States.

Duan J. & He J. 2011: Distribution and isotopic composition of *n*-alkanes from grass, reed, and tree leave along a latitudinal gradient in China. *Geochemical Journal* 45, 199–207. https://doi.org/10.2343/geochemj.1.0115

Fabiańska M.J. & Kurkiewicz S.2013: Biomarkers, aromatic hydrocarbons and polar compounds in the Neogene lignites and gangue sediments of the Konin and Turoszów Brown Coal Basins (Poland). *International Journal of Coal Geology* 107, 24–44. https://doi.org/10.1016/j.coal.2012.11.008

Ficken K.J., Li B., Swain D.L. & Eglinton G. 2000: An *n*-alkane proxy for the sedimentary input of submerged/floating freshwater aquatic macrophytes. *Organic Geochemistry* 31, 745–749. https://doi.org/10.1016/S0146-6380(00)00081-4

Fu X., Wang J., Chen W., Feng X., Wang D., Song C. & Zeng S. 2015: Elemental geochemistry of the early Jurassic black shales in the Qiangtang Basin, eastern Tethys: constraints for paleoenvironment conditions. *Journal of Geology* 51, 443–454. https://doi.org/10.1002/gj.2642

Hautevelle Y., Michels R., Malartre F. & Trouiller A. 2006: Vascular plant biomarkers as proxies for palaeoflora and palaeoclimatic changes at the Dogger/Malm transition of the Paris Basin (France). *Organic Geochemistry* 37, 610–625. https://doi.org/10.1016/j.orggeochem.2005.12.010

Huang X., Xue J., Wang X., Meyers P.A., Huang J. & Xie S. 2013: Paleoclimate influence on early diagenesis of plant triterpenes in the Dajiuhu peatland, central China. *Geochimica et Cosmochimica Acta* 123, 106–119. https://doi.org/10.1016/j.gca.2013.09.017

Ivanov D., Utescher, T., Mosbrugger V., Syabryaj S., Djordjević-Milutinović D. & Molchanoff S. 2011: Miocene vegetation and climate dynamics in Eastern and Central Paratethys (Southeastern Europe). *Palaeogeography, Palaeoclimatology, Palaeoecology* 304, 262–275. https://doi.org/10.1016/j.palaeo.2010.07.006

Jiamo F., Guojyng S., Jiayou X., Eglinton G., Gowar A.P., Rongfren J., Shanfa F. & Pingan P. 1990: Application of biological markers in the assessment of paleoenvironments of Chinese non-marine sediments. *Organic Geochemistry* 16, 769–779. https://doi.org/10.1016/0146-6380(90)90116-H

Jiang Z. & Fowler M.G. 1986: Carotenoid-derived alkanes in oils from northwestern China. *Organic Geochemistry* 10, 831–839. https://doi.org/10.1016/S0146-6380(86)80020-1

Jiménez-Moreno G., Fauquette S. & Suc J.P. 2008: Vegetation, climate and palaeoaltitude reconstructions of the Eastern Alps during the Miocene based on pollen records from Austria, Central Europe. *Journal of Biogeography* 35, 1638–1649. https://doi.org/10.1111/j.1365-2699.2008.01911.x

Kalkreuth W., Keuser C., Fowler M., Mcintyre M.L.P.D., Püttmann W. & Richardson R. 1998: The petrology, organic geochemistry and palynology of Tertiary age Eureka Sound Group coals, Arctic Canada. *Organic Geochemistry* 29, 799–809. https://doi.org/10.1016/S0146-6380(98)00122-3

Kováč M., Andreyeva-Grigorovich A., Barjaktarević Z., Brzobohatý R., Filipescu S., Fodor L., Harzhauser M., Nagymarosy A., Oszczypko N., Pavelić D., Rögl F., Saftić B., Silva L. & Studencka B. 2007: Badenian evolution of the Central Paratethys Sea: paleogeography, climate and eustatic sea-level changes. *Geologica Carpathica* 58, 579–606.

Krstić N., Savić Lj. & Jovanović G. 2012. The Neogene Lakes on the Balkan Land. *Annales Géologiques de la Péninsule Balkanique* 73, 37–60. https://doi.org/10.2298/GABP1273037K

Larcher A.V., Alexander R. & Kagi R.I. 1987: Changes in configuration of extended moretanes with increasing sediment maturity. *Organic Geochemistry* 11, 59–63. https://doi.org/10.1016/0146-6380(87)90027-1

Leventhal J.S. 1987: Carbon and sulfur relationship in Devonian shales from the Appalachian Basin as an indicator of environment of deposition. *American Journal of Science* 287, 33–49. https://doi.org/10.2475/ajs.287.1.33

Liu G. & Zhou D. 2007: Application of microelements analysis in identifying sedimentary environment: Taking Qianjiang Formation in the Jianghan Basin as an example. *Petroleum Geology & Experiment* 29, 307–314.

LKSD-1 2003: Lake Sediments Reference Materials LKSD-1 to LKSD-4, Lake Sediment. *CANMET Mining and Mineral Science Laboratories*, Canada.

LKSD-3 2003: Lake Sediments Reference Materials LKSD-1 to LKSD-4, Lake Sediment. *CANMET Mining and Mineral Science Laboratories*, Canada.

Lone A.M., Fousiya A.L., Rayees Shah A.A. & Achyuthan H. 2018: Reconstruction of Paleoclimate and Environmental Fluctuations Since the Early Holocene Period Using Organic Matter and C:N

Proxy Records: A Review. *Journal of the Geological Society of India* 91, 209–214. https://doi.org/10.1007/s12594-018-0837-6

Lüniger G. & Schwark L. 2002: Characterisation of sedimentary organic matter by bulk and molecular geochemical proxies: an example from Oligocene maar-type Lake Enspel, Germany. *Sedimentary Geology* 148, 275–288. https://doi.org/10.1016/S0037-0738(01)00222-6

Malešević M., Vukanović M., Obradinović Z., Dimitrijević M., Brković T., Stefanović M., Stanisavljević R., Jovanović O., Trifunović S., Karajičić LJ., Jovanović M. & Pavlović Z. 1974: Explanation to the Basic Geologic Map of Serbia, section K34-31 (Kuršumlija). *Federal Geological survey*, Belgrade (in Serbian). http://geoliss.mre.gov.rs/OGK/RasterSrbija/ (accessed March 10, 2018).

Meyers P. & Ishiwatari R. 1993: Lacustrine organic geochemistry – an overview of indicators of organic matter sources and diagenesis in lake sediments. *Organic Geochemistry* 20, 867–900. https://doi.org/10.1016/0146-6380(93)90100-P

Meyers P. & Lallier-Vergès E. 1999: Lacustrine sedimentary organic matter records of Late Quaternary paleoclimates. *Journal of Paleolimnology* 21, 345–372. https://doi.org/10.1023/A:1008073732192

Nakamura H., Sawada K. & Takahashi M. 2010: Aliphatic and aromatic terpenoid biomarkers in Cretaceous and Paleogene angiosperm fossils from Japan. *Organic Geochemistry* 41, 975–980. https://doi.org/10.1016/j.orggeochem.2010.03.007

NCS FC 28009L 2016: Certificate of Certified Reference Material, Coal. *China National Analysis Center for Iron and Steel*, China.

Otto A. & Wilde V. 2001: Sesqui-, di- and triterpenoids as chemosystematic markers in extant conifers – A review. *The Botanical Review* 67, 141–238. https://doi.org/10.1007/BF02858076

Pavlović M. 1969: Miozän-säugetiere des Toplica-beckens – paläontologisch-stratigraphische Studie. *Annales Géologiques de la Péninsule Balkanique* 34, 269–394. https://doi.org/10.2298/GABP6934269P

Perišić S., Jocić M., Karadžić B. & Djurdjević L. 2004: The forest melliferous flora in the vicinity of Blace (Serbia). *Archives of Biological Sciences* 56, 39–44. https://doi.org/10.2298/ABS0402039P

Peters K.E. 1986: Guidelines for Evaluating Petroleum Source Rock Using Programmed Pyrolysis. *AAPG Bulletin* 70, 318–329. https://doi.org/10.1306/94885688-1704-11D7-8645000102C1865D

Peters K.E. & Moldowan J.M. 1991: Effects of source, thermal maturity, and biodegradation on the distribution and isomerization of homohopanes in petroleum. *Organic Geochemistry* 17, 47–61. https://doi.org/10.1016/0146-6380(91)90039-M

Peters K.E., Walters C. & Moldowan J.M. 2005: The Biomarker Guide: I. Biomarkers and Isotopes in the Environment and Human History. *University Press*, Cambridge, 1–471.

Piller W., Harzhauser M. & Mandic O. 2007: Miocene Central Paratethys Stratigraphy – Current Status and Future Directions. *Stratigraphy* 4, 151–168.

Schulte S., Mangelsdorf K. & Rullkötter J. 2000: Organic matter preservation on the Pakistan continental margin as revealed by biomarker geochemistry. *Organic Geochemistry* 31, 1005–1022. https://doi.org/10.1016/S0146-6380(00)00108-X

Randazzo A., Müller P., Lelkes G., Juhász E. & Hámor T. 1999: Cool-water limestones of the Pannonian basinal system, Middle Miocene, Hungary. *Journal of Sedimentary Research* 69, 283–293. https://doi.org/10.2110/jsr.69.283

RS RHMZ. Meteorološki Godišnjak 1, klimatološki podaci 2019. *Republika Srbija, Republički hidrometeorološki zavod*, Belgrade (in Serbian). http://www.hidmet.gov.rs/ (accessed 20 December 2020).

Schwark L. & Empt P. 2006: Sterane biomarkers as indicator of Palaeozoic algal evolution and extinction events. *Palaeogeography, Palaeoclimatology, Palaeoecology* 240, 225–236. https://doi.org/10.1016/j.palaeo.2006.03.050

Seifert W.K. & Moldowan J.M. 1980: The effect of thermal stress on source-rock quality as measured by hopane stereochemistry. *Physics and Chemistry of the Earth* 12, 229–237. https://doi.org/10.1016/0079-1946(79)90107-1

Sinninghe Damasté J.S., Keing F., Koopmans M.F., Koster J., Schouten S., Hayes J.M. & de Leeuw J.W. 1995: Evidence for gammacerane as an indicator of water column stratification. *Geochimica et Cosmochimica Acta* 59, 1895–1900. https://doi.org/10.1016/0016-7037(95)00073-9

Soclo H.H., Garrigues P.H. & Ewald M. 2000: Origin of polycyclic aromatic hydrocarbons (PAHs) in coastal marine sediments: case studies in Cotonou (Benin) and Aquitaine (France) areas. *Marine Pollution Bulletin* 40, 387–396. https://doi.org/10.1016/S0025-326X(99)00200-3

Soma Y., Tanaka A., Soma M. & Kawai T. 1996: Photosynthetic pigments and perylene in the sediments of southern basin of Lake Baikal. *Organic Geochemistry* 24, 553–561. https://doi.org/10.1016/S0146-6380(98)00056-4

Tissot B.P. & Welte D.H. 1984: Petroleum Formation and Occurrence. *Springer*: Heidelberg.

Utescher T., Djordjevic-Milutinovic D., Bruch A. & Mosbrugger V. 2007a: Palaeoclimate and vegetation change in Serbia during the last 30 Ma. *Palaeogeography, Palaeoclimatology, Palaeoecology* 253, 157–168. https://doi.org/10.1016/j.palaeo.2007.03.037

Utescher T., Erdei B., François L. & Mosbrugger V. 2007b: Tree diversity in the Miocene forests of Western Eurasia. *Palaeogeography, Palaeoclimatology, Palaeoecology* 253, 226–250. https://doi.org/10.1016/j.palaeo.2007.03.041

Vandenbroucke M. & Largeau C. 2007: Kerogen origin, evolution, and structure. *Organic Geochemistry* 38, 719–833. https://doi.org/10.1016/j.orggeochem.2007.01.001

Wen Z., Ruiyong W., Radke M., Qingyu W., Guoying S. & Zhili L. 2000: Retene in pyrolysates of algal and bacterial organic matter. *Organic Geochemistry* 31, 757–762. https://doi.org/10.1016/S0146-6380(00)00064-4

Xie G., Shen Y., Liu S. & Hao W. 2018: Trace and rare earth element (REE) characteristics of mudstones from Eocene Pinghu Formation and Oligocene Huagang Formation in Xihu Sag, East China Sea Basin: implications for provenance, depositional conditions and paleoclimate. *Marine and Petroleum Geology* 92, 20–36. https://doi.org/10.1016/j.marpetgeo.2018.02.019

Xu H., George S. & Hou D. 2019: Algal-derived polycyclic aromatic hydrocarbons in Paleogene lacustrine sediments from the Dongying Depression, Bohai Bay Basin, China. *Marine and Petroleum Geology* 102, 402–425. https://doi.org/10.1016/j.marpetgeo.2019.01.004

Zhang M., Dia S., Du B., Ji L. & Hu S. 2018: Mid-Cretaceous Hothouse Climate and the Expansion of Early Angiosperms. *Acta Geologica Sinica* 92, 2004–2025. https://doi.org/10.1111/1755-6724.13692

Electronic supplementary material is available online at:
http://geologicacarpathica.com/data/files/supplements/GC-72-5-Burazer_Supplement.pdf